Original article

Discovery of anxiolytic 2-ferrocenyl-1,3-thiazolidin-4-ones exerting GABA$_A$ receptor interaction *via* the benzodiazepine-binding site

Anka Pejović [a], Marija S. Denić [b], Dragana Stevanović [a], Ivan Damljanović [a], Mirjana Vukićević [c], Kalina Kostova [d], Maya Tavlinova-Kirilova [d], Pavle Randjelović [e], Nikola M. Stojanović [f], Goran A. Bogdanović [g], Polina Blagojević [b], Matthias D'hooghe [h], Niko S. Radulović [b, *], Rastko D. Vukićević [a, **]

[a] *Department of Chemistry, Faculty of Science, University of Kragujevac, R. Domanovića 12, 34000 Kragujevac, Serbia*
[b] *Department of Chemistry, Faculty of Science and Mathematics, University of Niš, Višegradska 33, 18000 Niš, Serbia*
[c] *Department of Pharmacy, Faculty of Medicinal Sciences, University of Kragujevac, S. Markovića 69, 34000 Kragujevac, Serbia*
[d] *Institute of Organic Chemistry with Centre of Phytochemistry, Bulgarian Academy of Sciences, Bl. 9, Acad. G. Bonchev Str., Sofia 1113, Bulgaria*
[e] *Department of Physiology, Faculty of Medicine, University of Niš, Bulevar Zorana Đinđića 81, 18000 Niš, Serbia*
[f] *Faculty of Medicine, University of Niš, Bulevar Zorana Đinđića 81, 18000 Niš, Serbia*
[g] *Vinča Institute of Nuclear Sciences, Laboratory of Theoretical Physics and Condensed Matter Physics, PO Box 522, 11001 Belgrade, Serbia*
[h] *SynBioC Research Group, Department of Sustainable Organic Chemistry and Technology, Ghent University, Coupure Links 653, B-9000 Gent, Belgium*

ARTICLE INFO

ABSTRACT

Herein, we report on the synthesis, spectral, crystallographic and electrochemical properties of a small library of *N*-substituted 2-ferrocenyl-1,3-thiazolidin-4-ones, designed as novel GABA$_A$ benzodiazepine-binding site ligands. The anxiolytic properties of the title compounds were evaluated in several different *in vivo* models, whereas the involvement of the GABA$_A$ receptor complex in the activity of the most potent compound, 2-ferrocenyl-3-(4-methoxyphenylethyl)-1,3-thiazolidin-4-one, was inferred from experiments with known GABA$_A$-targeting agents. Ligand docking experiments revealed that the high, dose-dependent, anxiolytic activity of the new compounds might be due to their favorable interactions with the benzodiazepine-binding site of the GABA$_A$ receptor complex. The incorporation of the ferrocene core and fine tuning of the distance between the thiazolidinone core and an additional aromatic ring were judged to be crucial structural requirements for the observed anxiolytic effect.

© 2014 Elsevier Masson SAS. All rights reserved.

1. Introduction

Since their discovery in the mid-1950s, drugs targeting the γ-aminobutyric acid A receptor (GABA$_A$ agonists; e.g., the family of benzodiazepine, BZD, compounds) have been and still are the first choice in the treatment of anxiety [1–4]. The fully functional GABA$_A$ receptor is a membrane-bound heteropentameric protein consisting of an assembly of different subunits (usually α, β and γ-subtypes; different subunit isoforms are possible), together forming a pore for chloride ion transport [4,5]. A number of GABA$_A$ agonists bind to an allosteric site (BZD-binding pocket) located on the GABA$_A$ receptor complex and exert a positive cooperative effect that results in increased frequency of chloride channel opening (there are other modulatory sites on the GABA$_A$ receptor, i.e. barbiturate, neuroactive steroid etc.) [4,5]. The flow of chloride ions causes excitation/depolarization, shunting or inhibition/hyperpolarization of neurons [6]. The development of novel compounds that target the GABA$_A$ system is driven by the need to improve the effectiveness and lessen the side effects of existing drugs [2]. In that sense, the aim of this study was the design and synthesis of a novel class of GABA$_A$-targeting anxiolytics. In that respect, a small library of 1,3-thiazolidin-4-one–ferrocene hybrids (*N*-substituted 2-ferrocenyl-1,3-thiazolidin-4-ones; 13 compounds in total) was designed on the following three premises: (*i*) Therapeutically speaking, besides as anxiolytics, GABA$_A$ agonists are frequently used as anticonvulsant, sedative-hypnotic, and muscle-relaxant drugs [4]. In recent years, there is a growing tendency towards the use of anticonvulsants as an alternative treatment for some

---

* Corresponding author.
** Corresponding author.
E-mail addresses: nikoradulovic@yahoo.com, vangelis0703@yahoo.com (N.S. Radulović), vuk@kg.ac.rs (R.D. Vukićević).

anxiety disorders in individuals who are partially responsive or nonresponsive to conventional therapy [1,7]. It was previously shown that certain 1,3-thiazolidin-4-one derivatives act as anticonvulsants [8–11]; however, their possible use as anxiolytic agents has not been pursued thus far. (*ii*) A number of studies have shown that the introduction of the ferrocene core (Fc), or a formal exchange of an existing aromatic ring with Fc, may significantly enhance a molecule's (desirable) bioactive properties [12–18]. For example, ferrocene analogues of the antimalarial drug chloroquine are active against chloroquine-resistant strains of *Plasmodium falciparum*; one of these, ferroquine, made it to clinical trials [19,20]. The Fc unit might act as a hydrophobic spacer and/or lipophilicity/bioavailability enhancer (enabling easier passage through cell membranes) [20]. It is also known that the ferrocene Fe^{2+}/Fe^{3+} redox chemistry might contribute to the bioactivity of ferrocene derivatives [21]. (*iii*) Despite possessing unique features, the library compounds isosterically resemble the known BZD-type anxiolytics (Fig. 1), *i.e.*, we hypothesized that they could fulfill known BZD-binding site requirements, and thus could potentially have a high affinity towards the GABA$_A$ receptor [22].

Anxiolytic properties of all library compounds were evaluated in several different *in vivo* models (light/dark, open field, horizontal wire and diazepam-induced sleep tests). The involvement of the GABA$_A$ receptor complex was assessed using the known GABA$_A$-targeting agents flumazenil (competitive antagonist), picrotoxin (GABA$_A$ channel blocker), pentylenetetrazol and isoniazid (convulsants). In order to rationalize the obtained experimental results and disclose structure–activity relationships, i.e., to gain insight into the possible interactions of the title compounds with the GABA$_A$ receptor (possible involvement of BZD-binding site), ligand docking experiments were performed based on the recently published unified $\alpha_1\beta_2\gamma_2$ GABA$_A$ receptor model (this is believed to be the most abundant receptor subtype) [23]. Alongside with these results, we present detailed data on the spectral and electrochemical properties, as well as the crystal structure of the studied heterocycle-organometallic hybrids.

2. Results and discussion

2.1. Library design

The starting point for the library design was the notion that 1,3-thiazolidin-4-ones, as is the case for GABA$_A$ agonists, are known to act as anticonvulsants [8–11]. However, their possible use as anxiolytic agents has not been explored previously. The idea was to prepare a series of 1,3-thiazolidin-4-one derivatives with key structural attributes of well-known GABA$_A$ agonists (BZD-type compounds).

We started from Cook's et al. pharmacophore/receptor model for agonists and inverse agonists at the GABA$_A$ (BZD-binding site) [22]. For example, the central structural features of the GABA$_A$ agonist diazepam (Fig. 1a), fitted into the mentioned model, is the 1*H*-1,4-diazepin-2(3*H*)-one core, which is fused to a chlorobenzene ring and bears a phenyl substituent. The hypothetical pharmacophore triangle is depicted in red (edges, angles and vertices of the triangle are defined in Fig. 1b). According to Cook's et al. model, potential GABA$_A$ agonists should be able to interact with the following (sub)sites of the receptor: (*i*) an H-bond acceptor (A$_2$), (*ii*) an H-bond donor (H$_1$), (*iii*) a 'bifunctional' hydrogen-bond donor/acceptor site (H$_2$/A$_3$), (*iv*) four lipophilic pockets (L$_1$, L$_2$, L$_3$, and LD$_i$), and (*v*) three sterically forbidden sites (S$_1$, S$_2$, and S$_3$) (Fig. 1a). Hydrogen-bond donor sites H$_1$ and H$_2$, hydrogen bond acceptor A$_2$
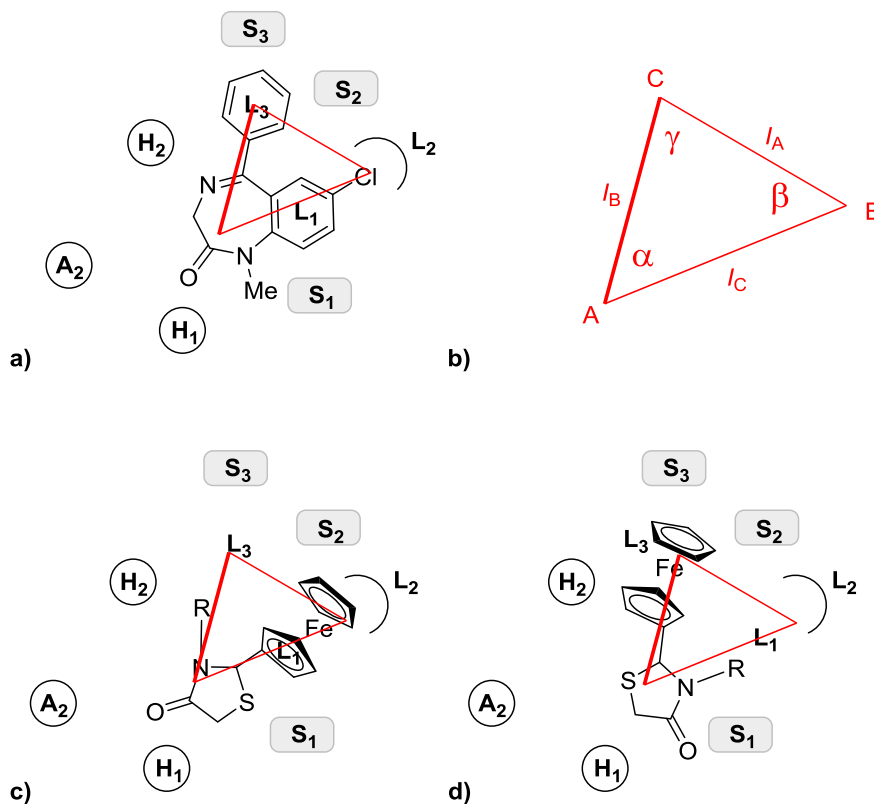
Fig. 1. a) Pharmacophore model [7] for the BZD-binding site of the GABA$_A$ receptor (A$_1$-A$_3$-H-bond acceptor, H$_1$, H$_2$–H-bond acceptor, S$_1$–S$_3$-sterically forbidden sites, L$_1$-L$_3$-lipophilic pockets), with diazepam as template; the hypothetical pharmacophore triangle is given in red. b) Edges (l_A, l_B, l_C), angles (α, β, γ) and vertices (A, B, C) of the hypothetical pharmacophore triangle. c) and d) Fitting of *N*-substituted 2-ferrocenyl-1,3-thiazolidin-4-ones into the proposed model for ligands targeting the GABA$_A$ complex. (For interpretation of the references to colour in this figure legend, the reader is referred to the web version of this article.)

and lipophilic region L_1 were assigned as four basic anchor points on the receptor protein-complex [22]. We believe that certain 1,3-thiazolidin-4-one derivatives should also be able to fit this model. We initially placed the thiazolidinone core at the position (vertex A) of the analogous heterocyclic moiety from the diazepam molecule ($1H$-1,4-diazepin-2($3H$)-one ring; Fig. 1c and d): the 1,3-thiazolidin-4-one carbonyl unit is a strong H-bond acceptor (possible interactions with H_1 receptor (sub)site), while the divalent sulfur atom could either act as a weak H-bond acceptor or eventually may form a favorable S—π interaction with the appropriate arene system at the receptor-binding site [24]. Now, we had to "expand" the molecule as to fit the pharmacophoric triangle. Thus, the 1,3-thiazolidin-4-one substitution pattern was chosen in a way to match, as closely as possible, the value of angle α, while the identity of the substituents had to comply with l_A, l_B, l_C (triangle edges), β and γ (triangle angles) values (Fig. 1b). We decided one of the substituents to be the ferrocene core, as we expected that it would nicely fit L_1/L_2 (Fig. 1c) or L_3 (Fig. 1d) lipophilic pockets and could possibly act as an "activity enhancer" [12—21]. Finally, we have chosen to vary the identity of the substituent attached to the nitrogen atom (R, Scheme 1), in order to gain an insight into possible SAR relationships. Two main types of R substituents were included in the study: aliphatic (n-alkyl chains of differing lengths, **3a—f**; "aliphatic analogues") and aromatic (with benzene/furan/thiophene cores, **3g—m**; "aromatic analogues"). Within the "aromatic" series (which might be more active, e.g. due to possible favorable π—π interaction), we have varied the length of the —$(CH_2)_n$— ($n = 0$—2) spacer between the N-atom and the aromatic core. This was done to finely tune l_A, l_B and l_C values, as well as to probe if higher conformational freedom of the molecule would influence the net activity. Another reason for the synthesis of **3i**, **3j** (heteroaromatics) and **3g** (methoxyphenyl group) was the fact that these compounds contain additional H-acceptors (S/O-atoms) that could increase the ligand's affinity towards the receptor.
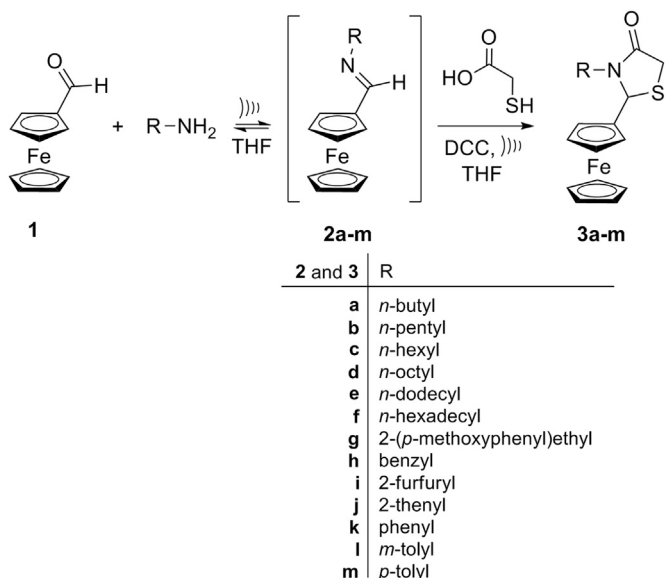
2.2. Chemistry

Among many reported protocols towards the synthesis of 1,3-thiazolidin-4-ones [11,25], the reaction of α-mercapto carboxylic acids with imines, known for more than sixty years [26,27], seems to be the most convenient one. The reaction employs readily available substrates and is easy to perform. There are three experimental variants of the synthesis: (*i*) Reaction of α-mercapto carboxylic acids with imines obtained in a separate experiment (as it had originally been conducted) [26]; this approach was previously employed in the synthesis of several 2-ferrocenyl-1,3-thiazolidin-4-ones, but the achieved yields were very poor (1.6—10.8%) [28]; (*ii*) A continuous process using a water separator and the same solvent for both steps (the synthesis of imines and their condensation with α-mercapto carboxylic acids) [27]; (*iii*) a one-pot three-component technique with the use of a suitable dehydrating agent [29—31]. We have chosen the latter, one-pot approach for the synthesis of the target N-substituted 2-ferrocenyl-1,3-thiazolidin-4-ones (**3a—m**). The method utilizes ferrocenecarboxaldehyde (**1**, FcCHO), an appropriate primary amine (**2a—m**), thioglycolic acid and DCC as a dehydrating agent in THF (Scheme 1). This approach was previously employed for the synthesis of analogous compounds [29,31], with the ratio of reactants being amine/aldehyde/mercapto acid = 1/2/3. However, in this case the yields based on the used aldehydes are necessarily less than 50%. This was not a reasonable approach in our case, since FcCHO (**1**) was the most valuable (expensive) reactant. Hence, we tried to improve the original protocol in order to achieve higher reaction yields with regard to FcCHO. We found that optimal results were obtained by a 25 min ultrasonic irradiation of the reaction mixture consisting of an amine, FcCHO and thioglycolic acid in the ratio 1/1/2. The corresponding N-substituted 2-ferrocenyl-1,3-thiazolidin-4-ones (**3a—m**, Scheme 1) were obtained in moderate-to-high yields, calculated by taking **1** as the limiting reagent (See Experimental section).

Compounds **3a—m** were spectroscopically characterized by IR, UV—Vis, MS, ^1H and ^{13}C NMR spectroscopy (see Experimental section and Supporting Information). The obtained spectral data agreed favorably with the expected structures for all compounds [15,17,32—37]. Several well-resolved IR bands associated with characteristic vibrations of the 2-ferrocenyl substituted 1,3-thiazolidin-4-one core—C=C stretching, Csp^2-H stretching, C=O stretching and the symmetrical deformation of the thiazolidinone CH_2 group (scissoring)—were observed for nearly all compounds [32]. An assortment of other bands, characteristic for the specific functional groups of individual compounds, were also observable in the corresponding spectra. For example, in the spectra of **3g**, **3h** and **3k—m**, the arrangements of the C—H out-of-plane bending bands in the 680—900 cm^{-1} region reflected the substitution patterns of the benzene ring, whereas the asymmetrical stretching and symmetrical deformation of the CH_3 group in N-alkyl and methoxy substituted compounds were observed as medium intensity bands around 2960 cm^{-1} and 1380 cm^{-1}, respectively.

In general, UV—Vis spectra of **3a—m** were marked by the presence of the ferrocene chromophore [18]. The band around 200 nm was the most intense one, assignable to $\pi \rightarrow \pi^*$ transitions, and was characteristic for the ferrocenyl moiety. The bands at *c.a.* 320 nm (although not noted in for all compounds) and 430 nm, which were about 100 times weaker than that at 200 nm, most probably corresponded to d $\rightarrow \pi^*$ and d—d transitions of the ferrocene core, respectively.

The ^1H NMR spectra contained typical signals for a mono-substituted ferrocene (dt (or m) at ~4.4 ppm, a multiplet at ~4.3 ppm and a singlet at ~4.2 ppm; last two signals were found to overlap occasionally) [18] and were also characterized by the presence of an ABX spin system formed by the methine (at ~5.34—5.90 ppm) and methylene protons (at ~3.60—3.81 ppm) of the thiazolidinone scaffold [33]. Generally speaking, when compared to the corresponding protons in 2,3-diaryl-1,3-thiazolidin-4-ones and 3-alkyl-2-aryl-1,3-thiazolidin-4-ones, the

Scheme 1. Synthesis of N-substituted 2-ferrocenyl-1,3-thiazolidin-4-ones (**3a—m**).

2 and 3	R
a	*n*-butyl
b	*n*-pentyl
c	*n*-hexyl
d	*n*-octyl
e	*n*-dodecyl
f	*n*-hexadecyl
g	2-(*p*-methoxyphenyl)ethyl
h	benzyl
i	2-furfuryl
j	2-thenyl
k	phenyl
l	*m*-tolyl
m	*p*-tolyl

ring methine and methylene protons were slightly shifted upfield by the presence of the ferrocene unit [33,34]. Similarly, signals at c.a. 85.0, 70.3, 69.7, 69.0, 68.5 and 67.7 ppm, observable in the ^{13}C NMR spectra of the library compounds, could be attributed to the ferrocene moiety [15] while the other characteristic signals, at about 169, 61 and 33 ppm were those corresponding to the carbonyl-, methine and methylene carbons of the thiazolidinone ring, respectively [35]. Depending on the nature of the substituent attached to the N-atom, other expected signals in both ^{1}H and ^{13}C NMR spectra were noted. Thus, in the spectra of **3g**, **3h** and **3k**−**m**, there were typical signals in the aromatic region, while the spectra of **3i** and **3j** contained characteristic signals of the thiophen-2-yl and furan-2-yl AMX systems.

The fragmentation pattern in the mass spectra of **3a**−**m** was a similar one to the previously reported for 2,3-diaryl-1,3-thiazolidin-4-ones, with the most striking differences relating to the base peak [36]. In the cases of **3a**−**m**, the base peak was the molecular ion as well; this suggests that the introduction of a ferrocene unit onto the thiazolidinone core increased the stability of corresponding [M]$^+$. Other characteristic ions observable in the MS spectra of **3a**−**m**, m/z 186 ([(C$_5$H$_5$)$_2$Fe]$^+$), 121 ([C$_5$H$_5$Fe]$^+$) and 56 ([Fe]$^+$), were those characteristic for a monosubstituted ferrocene derivative [37]. Moreover, in spectra of almost all compounds, the second most intense peak corresponded to a [FcCHNHR]$^+$ ion. Additional abundant ions in the mass spectra of N-aryl or N-arylalkyl derivatives were formed by scission of the C−N bond (eg. [C$_6$H$_5$]$^+$ at m/z 77 for **3k**, or [C$_7$H$_7$]$^+$ at m/z 91 for **3h**).

2.3. Crystallographic analysis

The structural features of thiazolidin-4-one **3k** as a representative example were also studied by a single-crystal X-ray structure analysis (Fig. 2 and Supporting Information). Two ferrocenyl Cp rings adopted an almost ideally eclipsed geometry with the C1−Cg1−Cg2−C6 torsion angle of only 0.2° (Cg1 and Cg2 are the centroids of the corresponding Cp rings; designations of the atoms are given on Fig. 2). However, the Cp rings slightly deviated from the parallel orientation (the dihedral angle between two the Cp rings was 4.0(2)°). The conformation of the thiazolidinone ring could be described as being close to an envelope, and the present orientation of the C14−C19 phenyl ring was influenced by an intramolecular C−H…π interaction between the C6−H6 group and the phenyl ring as a π-acceptor (Fig. 1). There were no classical H-bonds and π…π intermolecular interactions in the crystal packing of **3k**.

The S1−C13 heterocyclic five-membered ring (thiazolidone core) is directly bound to the C1−C5 cyclopentadiene ring via a single bond (C1−C11) with a bond distance of 1.504 (3) Å. However, the longest C−C bond in the crystal structure of **3k** was the C12−C13 bond, situated within the heterocyclic ring, while the remaining C−C bonds had π-character (Table 1). The S1 atom forms two S−C bonds which are significantly different in bond length, 1.849 (2) and 1.796 (3) Å for the S1−C11 and S1−C13, respectively. Around the sulfur atom, the C11−S1−C13 angle was considerably smaller than the rest of bond angles within the S1−C13 five-membered ring (Table 1). The sum of bond angles around N1 (359.8°) indicates trigonal geometry, i.e. sp^2 hybridization of N1.

The conformation of the thiazolidinone ring could be described as being close to an envelope since the C11, N1, C12 and C13 atoms were nearly coplanar (root-mean-square deviation from a mean plane of the fitted atoms was only 0.032 Å). The S1 atom was displaced from the C11−N1−C12−C13 mean plane by 0.622 (4) Å. The present ring conformation was also in agreement with the bond character of N1−C12 since this bond is the only one (within the ring) which had π-character and consequently forced a coplanar position of the C11, N1, C12 and C13 atoms. The dihedral angle between the C11−N1−C12−C13 plane and the C14−C19 phenyl ring was 58.57 (8)°. However, it seems that the present orientation of the C14−C19 phenyl ring was influenced by an intramolecular C−H … π interaction between the C6−H6 group and the phenyl ring as a π-acceptor (Fig. 1). A perpendicular distance of the H6 on the phenyl ring was only 2.74 Å (H6 … Cg = 2.80 Å, C6−H6 … Cg = 131°). The dihedral angle between the phenyl and the C6−C10 cyclopentadiene rings of 69.4 (1)° was also in agreement to the existence of this intramolecular interaction. Thus this C−H … π was the only apparent intramolecular interaction in the crystal structure of **3k** and it probably additionally stabilized the present molecular conformation.

There were no classical H-bonds in the crystal packing of **3k**. The reason for this could be found in the fact that molecules of **3k** do not possess any significant H-bond donors, such as O−H or N−H (Fig. 3 and S1). The C12−O1 carbonyl group may be recognized as the best H-bond acceptor in **3k** but it formed only a single weak hydrogen bond (C15−H15 … O1, Figure S1, Supporting Information) with H … O distance shorter than 2.60 Å. Although **3k** is comprised of three aromatic rings, it is interesting to note that this molecule did not form any π … π intermolecular interactions. The C6−C10
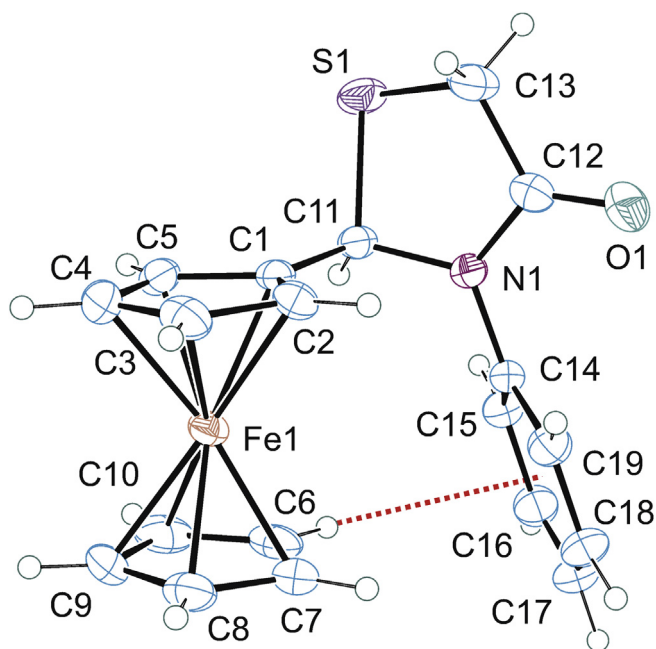

Fig. 2. Perspective view of **3k** with the atom-numbering scheme. Displacement ellipsoids are drawn at 40% probability level. The C6−H6…π intramolecular interaction is represented by a dotted red line. (For interpretation of the references to colour in this figure legend, the reader is referred to the web version of this article.)

Table 1
Selected bond lengths (Å) and bond angles (°) in the crystal structure of **3k**.

Bonds (Å)		Angles (°)	
S1−C13	1.796 (3)	C13−S1−C11	90.69 (11)
S1−C11	1.840 (2)	C12−N1−C14	122.4 (2)
O1−C12	1.215 (3)	C12−N1−C11	117.0 (2)
N1−C12	1.360 (3)	C14−N1−C11	120.42 (18)
N1−C14	1.437 (3)	N1−C11−S1	103.52 (14)
N1−C11	1.464 (3)	N1−C12−C13	111.4 (2)
C1−C11	1.504 (3)	C12−C13−S1	107.04 (18)
C12−C13	1.513 (4)		
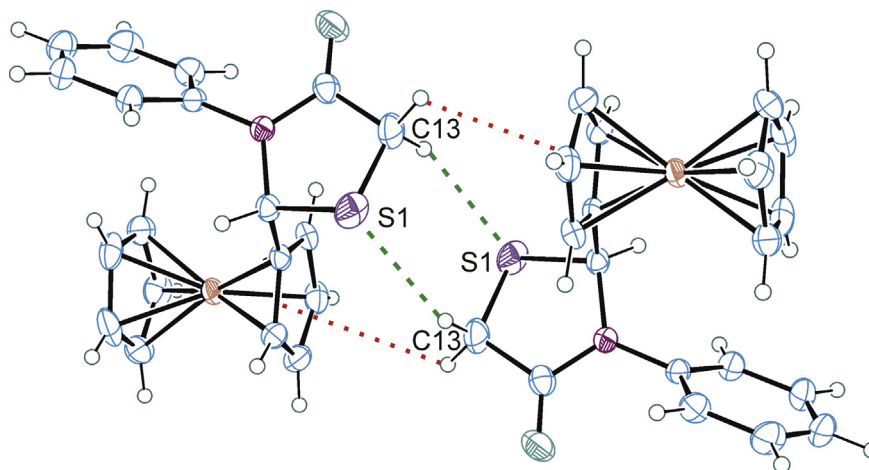
Fig. 3. The centrosymmetric dimer of **3k** formed *via* two C13−H13b … S1 (dashed green lines) and two C13−H13a … π (dotted red lines) intermolecular interactions. (For interpretation of the references to colour in this figure legend, the reader is referred to the web version of this article.)
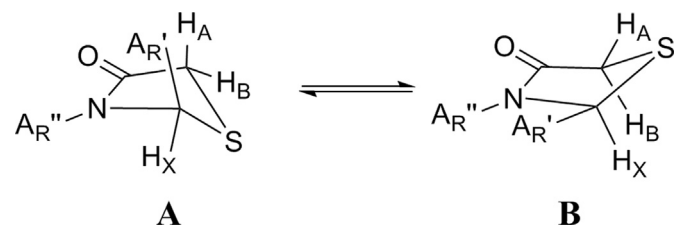
unsubstituted Cp ring participated in an intermolecular C−H … π interaction as a π-acceptor (Figure S2, Supporting Information) while the C14−C19 phenyl ring contributed to the same interaction as a C−H donor.

Probably the most interesting association of the molecules of **3k** in solid state was the formation of centrosymmetric dimers. Namely, two molecules within the dimer (Fig. 3) were interconnected by four interactions, two C−H … S and two C−H … π. Although these interactions are considered weak, their cumulative effect and the fact that two molecules are in a centrosymmetric arrangement most likely resulted in such stable dimers.

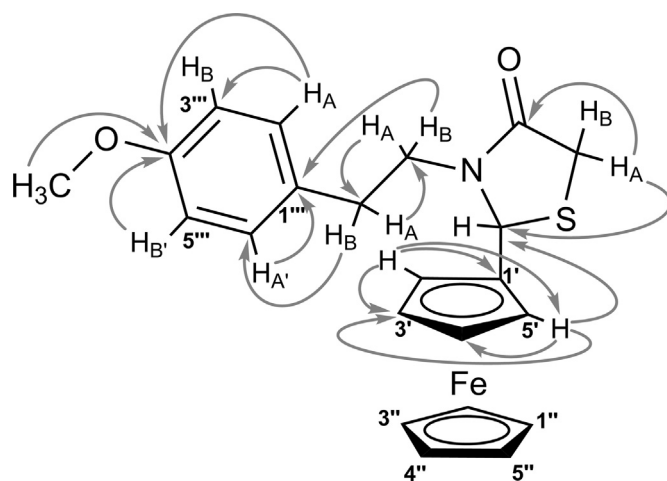### 2.4. Conformational analysis

In line with the results of the crystallographic analysis of **3k**, previous NMR and X-ray studies of 2,3-diaryl-1,3-thiazolidin-4-ones have showed that the favorable geometry of the heterocyclic ring corresponds to an envelope conformation, with the out-of-plane sulfur atom (conformations **A** and **B**, Fig. 4). Such geometry minimizes strain within the ring and ensures co-planarity of the carbonyl group and the *N*-aryl system (the latter enabling effective overlap of the corresponding orbitals). It was previously established that conformer **A** (Fig. 4), with a pseudo-axial C2 aryl substituent (A$_R$'), represented the preferred solid-state geometry, while conformer **B** (pseudo-equatorial A$_R$', Fig. 4) was the dominant one in solution [34,38]. This is in agreement with the crystal structure of **3k**.
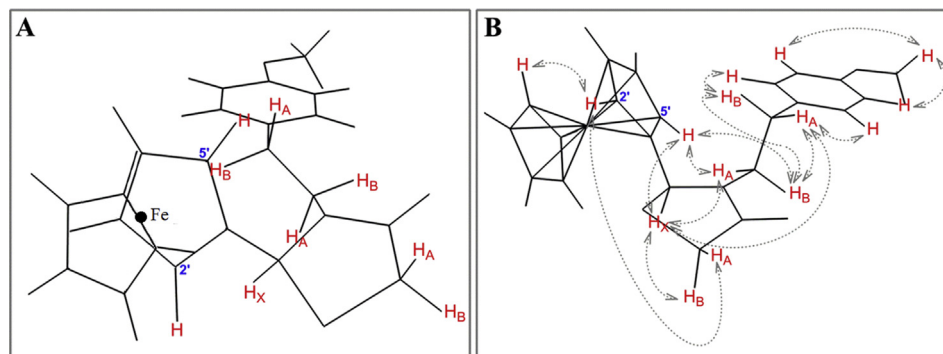
In order to explore the solution conformation (most probably that connected to the activity of the compounds) of our library compounds and to compare it to previous conformational features of 1,3-thiazolidin-4-one derivatives [34,38], we have performed a detailed 1D/2D NMR spectral study (DEPT, HSQC, HMBC (Fig. 5),

^{1}H−^{1}H COSY and NOESY) of **3a-m**, suggesting that the geometry with the pseudo-axial H_X (conformer **B**, Figs. 4 and 6) was the preferred one in solution as opposed to the solid-state one (see also Supporting Information). The results obtained for compound **3g** are summarized in Table 2, and Figs. 5 and 6. The use of higher magnetic field (400 MHz) and DMSO-d_6 as deuterated solvent enabled a clear resolution of the ABX splitting pattern of the thiazolidinone methine (C2H$_X$) and methylene protons (C5H$_A$H$_B$) (Table 2). The larger in value (in comparison to H_B) coupling of the methine proton H_X with the methylene proton H_A, appearing at lower field, indicated that these protons should be mutually *anti*-oriented. At the same time, the methine proton showed a nOe crosspeak with the upperfield methylene proton (and *vice versa*), suggesting that H_X and H_B are spatially near one to another. Based on the calculated **A** and **B** geometries of **3g** (MM + force field), the distances of H_X−C5H$_B$ in **A** (more than 4 Å) and **B** (around 3 Å) differed significantly in value (Fig. 6). This suggested that the geometry with the pseudo-axial H_X (conformer **B**, Figs. 4 and 6) was the preferred one in solution as opposed to the solid-state one; otherwise, one would expect the H_X−H_B nOe crosspeak not to appear. Furthermore, the ferrocene proton H5′ should be considerably closer to the N−CH$_2$ (*ca.* 2 Å) than to the Ar−CH$_2$ (*ca.* 4 Å) protons in conformer **B**, while the opposite should be true for conformer **A**. Thus, the fact that H5′

Fig. 4. 2,3-Diaryl-1,3-thiazolidin-4-ones conformers.

Fig. 5. Important HMBC interactions of **3g**.

Fig. 6. Preferred solid-state (**A**) and solution (**B**) conformers of **3g**, minimized using MM + force field. Important NOESY interactions are also shown on conformer **B**. Notation of some atoms, double and C–Fe bonds (conformer **A**) are omitted for clarity.

proton showed nOe crosspeaks with N–CH₂, but did not interact with Ar–CH₂ protons, corroborated the assumption that **B** was the preferred **3g** geometry in solution (Fig. 6).

There are two more pairs of diastereotopic protons in **3g** left unassigned. The protons of the CH₂ directly attached to nitrogen were shifted slightly downfield when compared to those next to the aromatic ring. A previous NMR study of 2-aryl-3-benzyl-1,3-thiazolidin-4-ones pointed to a large chemical shift difference (of approximately 1.5 ppm) between diastereotopic benzylic protons and the downfield shift of one of the protons was explained by stronger hydrogen bonding, as well as to hindered rotation around the N- and benzyl C-bond [34]. A similar trend was visible in the spectra of the herein studied benzyl (**3h**), 2-furfuryl (**3i**) and 2-thenyl (**3j**) derivatives, with the mentioned shift differences of about 1.1 ppm for the geminal N–CH₂ protons. The shift difference for the corresponding protons in **3g** was considerable lower (0.37 ppm), suggesting a higher degree of conformational freedom with respect to rotation about the N–C bond in **N–C**H₂CH₂.

2.5. Electrochemistry

As mentioned above, the Fe^{2+}/Fe^{3+} redox chemistry is known to contribute to the bioactivity of ferrocene derivatives [18]. Because of this, we decided to evaluate the electrochemical properties of the new compounds **3a–m**. This was done by means of cyclic

Table 2
^1H NMR (DMSO-d_6, 400 MHz) and ^{13}C NMR (DMSO-d_6, 100 MHz) data for **3g** (atom labels can be found in Fig. 5).

Position	^1H NMR	^{13}C NMR
1′	/	85.5
2′	4.42 (m, 1H)	67.2
3′	4.34–4.31 (m, 2H) – overlapped	68.3
4′		69.4
5′	4.49 (dt, J = 2.4, 1.4, 1.4 Hz, 1H)	70.2
1″, 2″, 3″, 4″ and 5″	4.24 (m, 5H)	68.7
1‴	/	130.4
2‴ and 6‴	6.99 (AA′BB′, J = 8.6 Hz, 2H)	129.4
3‴ and 5‴	6.82 (AA′BB′, J = 8.6 Hz, 2H)	113.8
4‴	/	157.7
N–CH$_A$H$_B$	3.34 (ddd, J = 13.6, 10.1, 5.8 Hz, 1H)	43.7
N–CH$_A$H$_B$	2.97 (ddd, J = 13.6, 9.8, 5.8 Hz, 1H)	43.7
CH$_A$H$_B$-Ar	2.60 (ddd, J = 13.2, 10.1, 5.8 Hz, 1H)	31.9
CH$_A$H$_B$-Ar	2.26 (ddd, J = 13.2, 9.8, 5.8 Hz, 1H)	31.9
S–CH$_A$H$_B$-C=O	3.61 (dd, J = 15.4, 1.6 Hz, 1H)	32.4
S–CH$_A$H$_B$-C=O	3.56 (dd, J = 15.4, 1.0 Hz, 1H)	32.4
N–CH–S	5.57 (br. s, 1H)	60.3
O–CH₃	3.71 (s, 3H)	54.9
C=O	/	169.5

voltammetry in acetonitrile containing 0.1 mol/L lithium perchlorate as the supporting electrolyte. Since preliminary measurements conducted with **3a** showed that this compound exhibits only a single redox couple ($E_{1/2}$ = +499 mV) in the potential range between −500 and +1000 mV (belonging to the ferrocene unit), we performed cyclic voltammetry experiments with all other compounds in the potential range between 0 and +1000 mV. It turned out that all thiazolidinones exhibit a reversible one-electron redox couple at a very similar potential ($E_{1/2}$ = +487 to +512, Table S1). Since the ferrocene unit of compounds **3a–m** is connected to an electron withdrawing group, these potentials are considerably more positive than that of the unsubstituted ferrocene. As representative examples, the voltammograms of **3a** and **3k** are depicted in Figure S3. Differences between anodic and cathodic peak potentials (Table S1) were close to the theoretical value; both anodic and cathodic peak currents were proportional to the square root of the scan rate (as illustrative examples graphs for **3a** and **3k** are given in Figure S4), and their ratio is independent of the scan rate, indicating a diffusion-controlled process.

2.6. Pharmacological studies

The synthesized thiazolidinone derivatives **3a–m** were evaluated for their CNS-modulating properties using the light/dark (LD), open field (OF), horizontal wire (HW) and diazepam-induced sleep tests. The results of the experiments are presented in Table 3 and Figure S5 (Supporting Information).

During the LD test, all library compounds increased the time mice spent in the brightly illuminated area, and decreased time spent in the dark one, in a dose-dependent manner (Table 3). However, **3g** was the only compound that significantly increased the number of crossings between the mentioned compartments at all applied doses, and in almost the same fashion as diazepam did. The effects of other library compounds drastically varied in the number of crossings and were dependent on the dose administered.

All of the tested compounds had increased (statistical significance) the latency of the first crossing from the illuminated compartment to the dark one (this referred to those groups that had transitions at all). This could be the result of an anxiolytic-like action of the thiazolidinone derivatives that is also a characteristic of benzodiazepines [39]. The increased latency of the first transition between compartments could be a reflection of the reduction of exploratory activity, which was observed for most of the herein studied compounds (the open field test). Nevertheless, this is a controversial parameter, commonly not discussed in studies on

Table 3
Effect of thiazolidinone derivatives **3a**–**m**, diazepam and vehicle on anxiety (LD test) and locomotor activity (OF test) in mice.

Compound	Dose (mg/kg)	Light/dark (LD) test			Open field (OF) test	
		Time spent in light box	No. of transitions	Time of the first transition	No. of squares crossed	No. of rearings
3a	25	204 ± 7^a	2.5 ± 0.5	39 ± 15^b	99 ± 11	6.4 ± 0.9^c
	50	218 ± 4^a	2.5 ± 0.2	42 ± 15^b	101 ± 9	4.4 ± 0.7
	100	285 ± 10^a	1.0 ± 0.5^b	195 ± 9^a	100 ± 9	3.9 ± 0.9
3b	25	199 ± 12^a	3.0 ± 0.2^a	47 ± 9^a	123 ± 9^a	6.9 ± 0.6^b
	50	224 ± 10^a	1.5 ± 0.2	106 ± 12^a	106 ± 9^c	5.8 ± 0.9
	100	289 ± 10^a	1.0 ± 0.2^a	164 ± 11^a	98 ± 9	5.5 ± 0.9
3c	25	203 ± 8^a	3.0 ± 0.8^c	37 ± 7^b	98 ± 10	5.2 ± 0.4
	50	219 ± 16^a	2.0 ± 0.5	68 ± 12^a	87 ± 11	5.0 ± 0.7
	100	292 ± 12^a	1.5 ± 0.2	94 ± 11^a	64 ± 10	4.2 ± 0.6
3d	25	213 ± 10^a	2.0 ± 0.5	46 ± 9^a	113 ± 12^b	8.0 ± 0.6^a
	50	223 ± 11^a	1.5 ± 0.2	42 ± 11^a	98 ± 9	6.8 ± 0.4^b
	100	300 ± 0^a	0 ± 0^a	0 ± 0^a	92 ± 2	4.5 ± 0.3
3e	25	220 ± 13^a	3.0 ± 0.2^a	51 ± 10^a	99 ± 15	5.7 ± 0.9
	50	231 ± 12^a	2.5 ± 0.2	63 ± 12^a	97 ± 10	5.2 ± 0.8
	100	294 ± 12^a	1.5 ± 0.5	89 ± 6^a	90 ± 11	4.8 ± 0.9
3f	25	193 ± 8^a	3.5 ± 0.5^a	72 ± 9^a	100 ± 9	5.5 ± 0.2
	50	213 ± 8^a	2.0 ± 0.5	$93 \pm 9.^a$	104 ± 10	5.1 ± 0.3
	100	276 ± 9^a	1.5 ± 0.2	101 ± 8^a	97 ± 13	4.9 ± 0.2
3g	25	144 ± 10^a	3.5 ± 0.8^b	56 ± 8^a	75 ± 16	12.4 ± 0.5^a
	50	224 ± 9^a	5.0 ± 0.5^a	61 ± 7^a	51 ± 13^c	14.0 ± 0.7^a
	100	257 ± 10^a	8.5 ± 0.8^a	74 ± 8^a	35 ± 10^a	15.5 ± 0.3^a
3h	25	271 ± 11^a	1.5 ± 0.2^c	84 ± 5^a	75 ± 16	2.3 ± 0.8
	50	300 ± 0^a	0 ± 0^a	0 ± 0^a	51 ± 13^c	3.6 ± 0.5
	100	300 ± 0^a	0 ± 0^a	0 ± 0^a	35 ± 10^a	5.1 ± 0.8
3i	25	221 ± 10^a	2.0 ± 0.2	89 ± 12^a	144 ± 3^a	7.2 ± 0.3^a
	50	277 ± 9^a	1.0 ± 0.5^b	106 ± 11^a	123 ± 10^a	8.1 ± 0.6^a
	100	300 ± 0^a	0 ± 0^a	0 ± 0^a	114 ± 9^b	8.6 ± 0.9^a
3j	25	207 ± 12^a	1 ± 1^c	57 ± 5^a	157 ± 11^a	8.3 ± 0.7^a
	50	300 ± 0^a	0 ± 0^a	0 ± 0^a	145 ± 7^a	9.5 ± 0.6^a
	100	300 ± 0^a	0 ± 0^a	0 ± 0^a	107 ± 8^c	10.1 ± 0.9^a
3k	25	132 ± 11^a	3.0 ± 0.2^a	54 ± 10^a	143 ± 12^a	7.4 ± 0.8^a
	50	194 ± 10^a	2.5 ± 0.2	64 ± 10^a	124 ± 14^a	6.7 ± 0.4^b
	100	279 ± 12^a	1.5 ± 0.5	71 ± 9^a	100 ± 10	5.4 ± 0.9
3l	25	121 ± 11^c	2.0 ± 0.2	44 ± 6^a	135 ± 15^a	8.7 ± 0.6^a
	50	175 ± 11^a	2.5 ± 0.2	50 ± 10^a	162 ± 12^a	9.5 ± 0.7^a
	100	267 ± 15^a	1.5 ± 0.5	99 ± 8^a	108 ± 13^c	5.3 ± 0.6
3m	25	117 ± 16	2.5 ± 0.2	32 ± 6^a	144 ± 11^a	8.5 ± 0.6^a
	50	181 ± 13^a	1.5 ± 0.8	63 ± 7^a	98 ± 10	6.6 ± 0.8^b
	100	300 ± 0^a	0 ± 0^a	0 ± 0^a	86 ± 15	2.4 ± 0.9
DZP	2	184 ± 12^a	10.5 ± 0.5^a	69 ± 3^a	145 ± 10^a	7.6 ± 3.1^a
VEH	10	99 ± 9	2.0 ± 0.25	16 ± 6	80 ± 21	4.1 ± 2.1

All substances (in the doses of 25, 50, 100 mg/kg for the experimental substances; DZP (2 mg/kg); Vehicle (VEH, 10 mL/kg)), were administrated 1 h prior to the experiment. Data are presented as mean $\pm$ SD, $n = 6$.
[a] $p < 0.001$; [b] $p < 0.01$; [c] $p < 0.05$ *vs.* vehicle.

experimental anxiety; compounds cause a decrease in locomotion and thus give false positive results [40].

To circumvent this situation, all new drugs are screened for nonspecific increases or decreases (aspects of sedation) in general locomotion in a novel arena (OF test). Anxiety behavior in rodents, observed during the OF test, is a consequence of individual (out of the group) testing of animals and agoraphobia. In these situations, rodents show a thigmotaxic behavior, identified by spontaneous preference for the periphery of the apparatus and reduced ambulation [41]. At lower doses, almost all tested substances increased the number of squares crossed in the OF apparatus (Table 3), whereas at higher doses a reversed effect was observed. This indicated the possible sedative/hypnotic or muscle relaxant effect of the library compounds. The impact on animal movement in the OF test depended on the structure of the group attached to the nitrogen atom. For example **3h**, with a benzyl group in the side chain, caused a suppression of the motor activity in the OF test even at low doses. The introduction of a heteroatom into the aromatic ring, as in **3i** and **3j**, resulted in an increase of locomotion in the lowest dose (25 mg/kg), although at higher doses the mentioned reversal of effect was noted. Elongation of the side chain with a methylene unit and the introduction of a methoxy group onto the

aromatic ring (**3g**) caused a dose-dependent increase in the number of squares crossed.

To rule out the possible muscle relaxant effect, mice were submitted to an HW test. All animals treated with thiazolidinone derivatives (at all doses) were capable of grasping a wire within the 10 s period (displaying 100% of activity), whereas diazepam (2 mg/kg; causing a failure to grasp in 50% of cases) decreased the ability of animals to grasp the wire (data not shown).

The observed depressant activity of **3a**–**m** during the OF suggested central mechanisms and not a peripheral neuromuscular blockade, as opposed to diazepam (at higher doses ≥ 10 mg/kg) that affects both mechanisms [42,43], as the library compounds did not exhibit a muscle relaxant activity even at doses as high as 100 mg/kg.

Strictly speaking, having all of this in mind and taking into account that the most reliable parameters for the assessment of anxiolytic drugs are the increase in time spent in the illuminated area, the number of crossings between light and dark compartments and increase of locomotion [44], under our experimental conditions, only substance **3g** could be regarded as possessing purely anxiolytic properties.

Because of the fact that the title compounds were designed to target the GABA$_A$ receptor, we decided to experimentally assess its
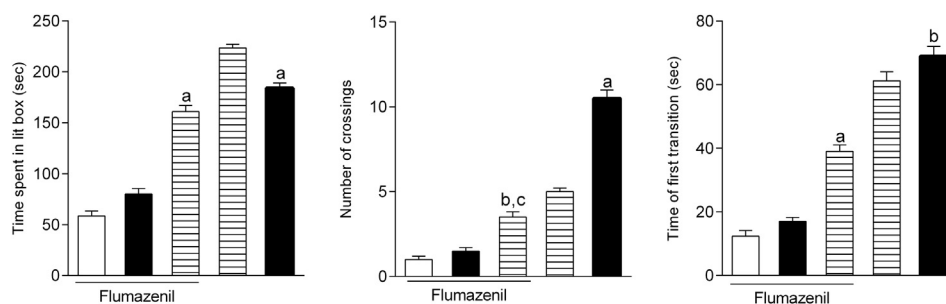
Fig. 7. Effect of vehicle (white column), diazepam (1 mg/kg; black column) and **3g** (50 mg/kg, striped column) following flumazenil (FLU; 3 mg/kg by ip) treatment on the time that the animals spent in the light compartment (first graph), on the number of crossings between compartments (second graph) and on the time of the first transition (third graph). Values are expressed as mean ± SD, $n = 6$, (a) $p < 0.0001$ vs. FLU + vehicle, FLU + diazepam and **3g**; (b) $p < 0.0001$ vs. FLU + vehicle, FLU + diazepam; (c) $p < 0.001$ vs. **3g**.
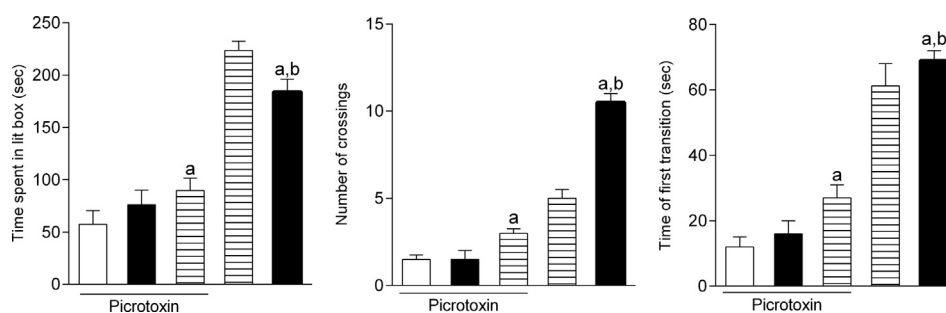
Fig. 8. Effect of vehicle (white column), diazepam (1 mg/kg; black column) and **3g** (50 mg/kg; striped column) following picrotoxin (PIC; 1 mg/kg by ip) treatment on the time that the animals spent in the light compartment (first graph), on the number of crossings between compartments (second graph) and on the time of the first transition (third graph). Values are expressed as mean ± SD, $n = 6$, (a) $p < 0.0001$ vs. PIC + vehicle and **3g**; (b) $p < 0.0001$ vs. PIC + diazepam.

possible involvement in the anxiolytic action of the library compounds. For this purpose, we have chosen **3g**, the most potent derivative with no CNS depressant or myorelaxant activity. We were additionally encouraged by the fact that **3g** and diazepam (GABA$_A$ agonist) displayed similar activity in the LD test. In order to evaluate the involvement of the GABA receptor, **3g** was further tested in the LD paradigm in combination with flumazenil (FLU, a competitive antagonist of GABA$_A$ receptor that antagonize both agonists and inverse agonists [45]) and picrotoxin (PIC, a noncompetitive GABA$_A$ receptor chloride channel antagonist (one can rather say channel blocker) [46]) (Figs. 7 and 8) and in pentylenetetrazol (PTZ)/isoniazid (INH)-induced convulsion tests (Table 4).

From Figs. 7 and 8, one can see that FLU and PIC, in both the vehicle and diazepam groups, produced an expected result: they decreased the time animals spent in the light compartment, decreased the number of crossings between compartments and decreased the time of the first transition. For the groups that received FLU/PIC and **3g**, the observed parameters were modified compared to the results of the animals that received **3g** alone, in the same dose (50 mg/kg). For example, the time that the animals from

group FLU+**3g** spent in the light compartment was decreased for almost a third of the time of animals from group **3g** (Fig. 7), whereas the time group PIC+**3g** animals spent in the light compartment was decreased for more than a half of the time of animals from group **3g** (Fig. 8). Likewise, the number of crossings between compartments and the time of the first transition were only partially reduced by FLU and PIC (but to a greater extent by PIC) when compared with the values noted for the animals from group **3g**. However, compound **3g** still displayed some degree of anxiolytic activity even in FLU and PIC pretreated animals (statistically significant differences existed between **3g** and vehicle pretreated groups). Also, statistically significant differences between groups that received the combination of FLU/PIC and **3g** and those that were administered with FLU/PIC and diazepam suggested the existence of additional effects that are probably due to other mechanisms involved in its anxiolytic action.

The hypnotic/sedative activity of the library compounds was estimated using the diazepam (20 mg/kg)-induced sleep model. Almost all substances had no significant effect on the onset of sleep, except for three compounds that caused a prolongation of this period (**3k**–**m**, having an aryl group directly attached to the

Table 4
Anticonvulsant effect of the vehicle (olive oil), **3g** and diazepam in the pentylenetetrazole (PTZ) − and isoniazid (INH) − induced seizures in mice.

Substance	Dose	PTZ		INH	
		Seizure onset (sec)	Onset of HLTE (sec)	Seizure onset (sec)	% of living mice in 30 min
Vehicle	10 mL/kg	39 ± 1	106 ± 10	1244 ± 26	0
3g	50 mg/kg	62 ± 2[a]	338 ± 14[a]	2207 ± 43[a]	100
Diazepam	1 mg/kg	601 ± 25[a]	1324 ± 38[a]	2197 ± 17[a]	100

Data are presented as mean ± SD, $n = 6$.
[a] $p < 0.001$ vs. vehicle.

nitrogen atom), but all of the tested library compounds significantly increased, in a dose-dependent manner, the duration of the sleep. These results suggested a central nervous system depressant activity and possible sedative properties of these thiazolidinone-ferrocene hybrids (Fig. S5). The tested hybrids had manifested a profound influence on the diazepam-induced sleep. Compounds **3a**−**f**, with an alkyl chain of variable length attached to the nitrogen atom, were the most active ones as they increased the sleeping period, in a dose-dependent manner, almost three-fold. The lowest effect was noted in the case of compound **3h** (which possesses a CH_2Ph group) treatment, where only its highest dose caused a statistically significant different prolongation of the diazepam-induced sleep. Once again the introduction of an oxygen or a sulfur atom (**3i** and **3j**) into the aromatic rings resulted in a significant alteration of activity. These sedative properties can be related to the activation of benzodiazepine and/or GABA sites of the GABA receptor complex. This is in accordance with a previous report on several thiazolidinone derivatives, tested at a dose of 100 mg/kg, that were found to potentiate the effect of a more general sedative, sleep-inducing agent (pentobarbital) [11]. The effects of sleep latency shortening and increase of total sleep time, as well as the enhancement of electroencephalogram power in the delta frequency range are some of the hypnotic drug characteristics (at higher doses) and it is considered to involve more pronounced depression of the CNS than sedation [47].

A matter that should be kept in mind when discussing the activity of our thiazolidinone derivatives is the differentiation of effects produced by benzodiazepine-type compounds binding to different GABA_A receptor subtypes (α_1, α_2 and α_3) [43]. The α_1 GABA_A receptor is known to mediate sedative, amnesic, and part of the anticonvulsant effects, while the α_2 GABA_A (and not α_3 GABA_A) receptor mediates the anxiolytic effects of diazepam. It was observed that α_2 GABA_A receptor (expressed on motor neurons and in the superficial layer of the dorsal horns) were primarily involved in the myorelaxant activity of diazepam, whereas at higher doses it was observed that α_3 GABA_A receptors are also included [43]. These results allow at least a partial explanation for the observed activity of the tested thiazolidinone-ferrocene hybrids. One can speculate that most of them possess higher affinity for α_1 GABA_A receptors (due to their activity in the OF and diazepam-induced sleep tests) than for α_2/α_3 GABA_A receptors that are involved in myorelaxant activity (negative results in HW test). For example, **3h** decreased the number of crossings in the OF test more than two folds when compared to the results of the vehicle pretreated animals (Table 3), but it did not modify the performance of mice in the HW test. It also prolonged, although not to a great extent, the diazepam-induced sleep (Figure S5, Supporting information). Furthermore, other compounds, such as **3i**, **3k** and **3m**, decreased the number of crossings in the OF test only at doses of 100 mg/kg, did not modify animal performance in the HW test, but prolonged the diazepam-induced sleep (two folds when compared to diazepam), also suggesting their higher affinity for α_1 GABA_A rather than for α_2 and α_3 GABA_A receptors.

Anticonvulsant effects of the library compounds were also studied in order to determine the possible interaction of **3g** with the GABA_A receptor complex. For that reason we utilized pentylenetetrazole (PTZ) and isoniazid (INH) that are known to interrelate with the GABA neurotransmitter itself and the GABA complex. PTZ not only produces epileptiform activity but also mimics the seizure induced behavioral changes that are very similar to temporal lobe epilepsy in humans and, thus, it has a predictive relevance regarding the clinical spectrum of activity of experimental compounds. It is also interesting to mention that neither PTZ nor INH-binding sites on GABA receptors belong to the GABA or PIC sites of the GABA receptor complex [48]. Compound **3g** exerted modest

activity (the results are presented in Table 4) compared to diazepam (1 mg/kg), but it significantly increased the convulsion threshold compared to vehicle pre-treated animals. These results further confirm the possible involvement of **3g** in signal transduction through GABA systems.

The used dose of **3g** (50 mg/kg) applied after a specific GABA_A antagonist could have been supramaximal and in this way could have masked its competitive effect for this receptor. Even after the application of a nonselective antagonist (PIC), **3g** exerted some degree of anxiolytic activity in the experimental animals suggesting that there are also other mechanisms involved in the activity of **3g**. The accumulated *in vivo* data regarding the possible interaction of the library compounds and the GABA_A receptor complex motivated us to perform *in silico* experiments that could provide further (pro/con) evidences for the proposed mechanism of action.

2.7. Molecular docking

The ligand-based [22] design of **3a**−**m** relied on the structure of GABA_A targeting BZD-type anxiolytics. In order to further explore whether the library compounds fit into the BZD-binding site and to possibly rationalize the results of *in vivo* experiments, we have decided to dock **3a**−**m**, as well as the appropriate standard drugs used in biological assays, into the extracellular domain of the GABA_A receptor (anxiolytic agents (usually) bind to this domain). Although the crystal structure for the GABA_A receptor is not yet available, there are several homology models that are in good agreement with experimental findings [23,49]. Among them, we have chosen a recently reported unified model of $\alpha_1\beta_2\gamma_2$ GABA_A receptor complex (the most abundant subunit combination), based on the glutamate-gated chloride ion channel (Fig. 9) [23]. The BZD-binding site is located on the extracellular surface of the receptor (Figs. 9 and 10) and it includes amino acid residues from 6 noncontiguous regions (these are usually designated as Loops A−F, Fig. 10A) of subunits α and γ [23,49]. For several classical benzodiazepines even specific amino acid residues that contribute to the binding are uncovered. For example, it is known that the molecule
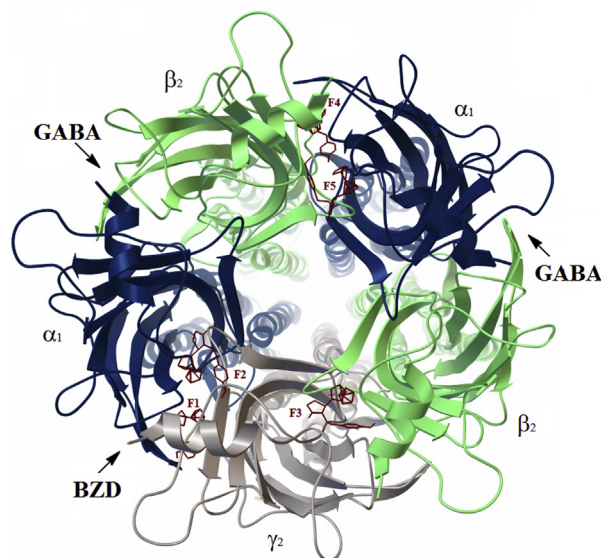
Fig. 9. Unified homology model of the GABA_A receptor complex [24] (the show perspective from the side of the receptor's extracellular domain). α_1, β_2 and γ_2 subunits are given in blue, green and gray, respectively; BZD- and GABA-binding sites are marked with arrows; the most favorable docking poses of **3g** are given in red (F1−F5 families of nodes). (For interpretation of the references to colour in this figure legend, the reader is referred to the web version of this article.)
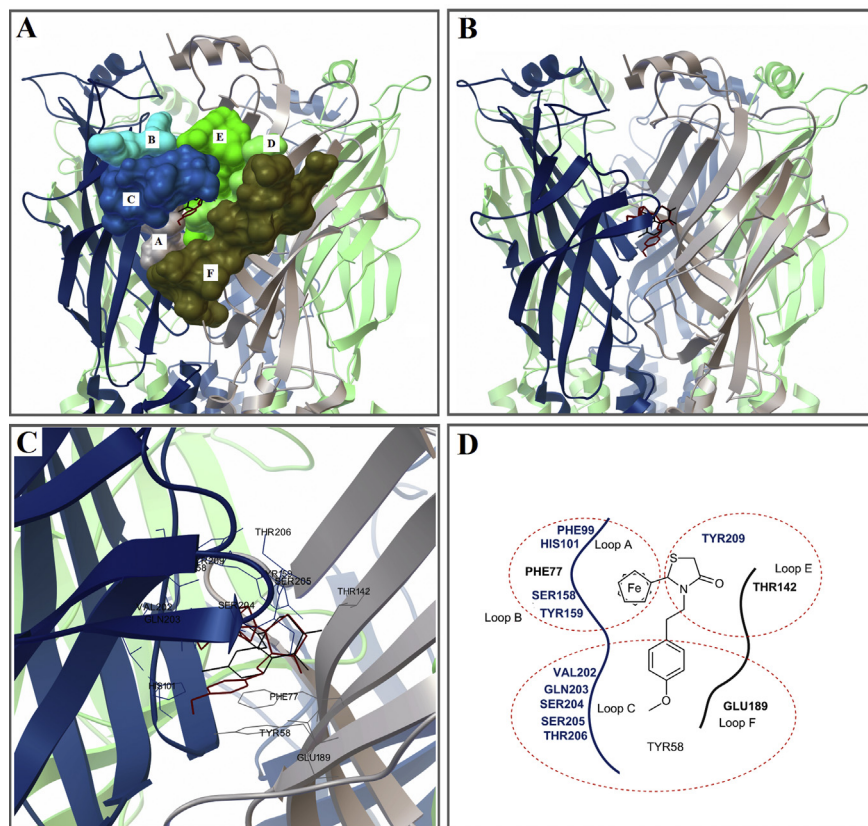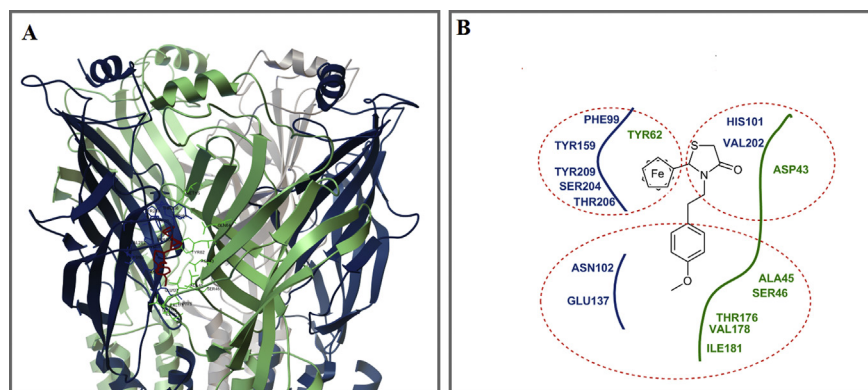
Fig. 10. The most preferred docking mode of **3g** at the BZD-binding site (F1): A − molecular surface of BZD pocket Loops A−F (Loop A − gray, Loop B − pale blue, Loop C − dark blue, Loop D − pale cyan, Loop E − bright green, Loop F − olive green); B − overlay of **3g** (solid red line) and diazepam (solid black line) at the BZD-binding site; C − amino acid residues found in the 4 Å-radius sphere around **3g** and diazepam, D − **3g** and the nearby amino acid residues (4 Å-radius sphere), a simplified representations (red dashed lines group spatially close entities). Color coding of the receptor subunits: α_1 (secondary structure, amino acid residues (C) or labels (D))-dark blue, γ_2 (secondary structure, amino acid residues and labels)-light gray, β_2 (secondary structure)-green. (For interpretation of the references to colour in this figure legend, the reader is referred to the web version of this article.)

of diazepam interacts with α_1His101, α_1Asn102 (Loop A), α_1Gly157 (Loop B), α_1Val202, α_1Ser205, α_1Thr206 and α_1Val211 (Loop C) [23,49].

All *in silico* experiments were performed as blind dockings, covering the entire extracellular domain of the receptor. We assumed that by limiting the search space to the BZD-binding pocket only we could lose valuable information on other possible favorable interactions between **3a**−**m** and the GABA$_A$ receptor, or could even get false "positive results"; it is known that several compounds (e.g. GABA (γ-aminobutyric acid), picrotoxin) do not

have a unique GABA$_A$ receptor binding site (Fig. 9) [50]. Additionally, blind docking also allowed validation of the docking experiments. Although the entire extracellular domain of the receptor was explored, the most favorable calculated pose for diazepam (binding energy −8.6 kcal/mol) was in agreement with the previous experimental findings (Fig. 10A−C). This mainly referred to the mutual spatial arrangement and the distance between diazepam and several α_1/γ_2 subunit amino acid residues, experimentally confirmed to be important for the binding. For example, α_1His101, α_1Asn102, α_1Val202, α_1Ser205, α_1Val211 "fell" within the 4 Å radius

Fig. 11. The most preferred F4-docking mode of **3g**: A−**3g** (solid red line) and the nearby amino acid residues (4 Å-radius sphere), B − a simplified representations of A (red dashed lines group spatially close entities). Color coding of the receptor subunits: α_1 (secondary structure, amino acid residues (A) or labels (B)) − dark blue, β_2 (secondary structure, amino acid residues and labels) − green, γ_2 (secondary structure) − light gray. (For interpretation of the references to colour in this figure legend, the reader is referred to the web version of this article.)

sphere around diazepam; the criteria that functional groups separated by less than 7 Å have the potential to interact, and that those within 4 Å may form salt bridges or hydrogen bonds, are generally accepted [23,49].

The main results of more than 150 individual docking experiments are summarized in Figs. 9–11, S6. With a few exceptions (which were not, energetically speaking, among the most favorable ones), all found binding modes for **3a**–**m** clustered them into five different families of poses (F1–F5; these designations will also be used for the appropriate regions of the receptor further on, Fig. 9). Modes belonging to F1 family (at the interface of α_1/γ_2 subunits) placed the molecules into the BZD-binding site (Fig. 9 and Fig. 10A–C). F2 modes were situated at the "top" of Loops B and E, while those from F3, and F4 and F5 families occupied pockets at the interface of α_1/β_2 and γ_2/β_2 subunits, respectively (Fig. 9). All docked compounds within all families had binding energies (for the search criteria, see Experimental section) from −6.0 to −9.2 kcal/mol. Nevertheless, in most cases, for a single compound, the best F1–F5 modes were mutually comparable and usually differed in less than 0.5 kcal/mol.

As discussed in previous subsections, the 2,3-disubstituted 1,3-thiazolidin-4-one ring is known to predominantly exist in one of the two different geometries (Fig. 4). Although AutoDock Vina [51] includes the possibility of a flexible dock (single bonds could be regarded as rotatable), it does not allow ring geometry to be changed. For this reason, the docking experiments (flexible ligands) were performed with two different input geometries of **3a**–**m** (these corresponded to the preferred solution and solid-state conformers). Generally speaking, the input geometry had (some) influence on the net docking results, but not as pronounced as one might expect. The same families of binding sites (F1–F5) were found for both input geometries, but the binding energies of the conformer pairs differed to some level. For example, mutual overlay of the best F1–F5 modes for compound **3g**, calculated starting from the two different input conformers (A and B, Fig. 4), are shown in Figure S6. It is interesting that, according to the calculated values of the corresponding binding energies, conformer B fitted better into F1–F3 regions of the receptor (Fig. 9), while geometry A showed more affinity towards F4/F5.

Except for **3d**, **3e** (aliphatic N-substituents) and **3k**–**m** (without a "spacer" between the N-atom and the aromatic core), the library compounds were successfully docked into the BZD-binding site (Fig. 10). According to the obtained results, compounds with a $(CH_2)_x$Ar substituent ($x = 1, 2$; "aromatic" analogues) attached to the N-atom should better interact with the GABA$_A$-BZD-binding pocket. The binding energy calculated for derivatives from the "aliphatic series" (**3a**–**c** and **3f**) ranged from −6.4 (**3f**) to −7.4 kcal/mol (**3a**), whereas for "aromatic" analogues (**3g**–**j**), it was found to be from −7.1 to −8.8 kcal/mol. In general, all of the docked compounds/geometries displayed a unique, energetically favorable F1-pose. Contrary to that, multiple different orientations of a single ligand were allowed within F2–F5 regions. This suggested that F2–F5 pockets were "too big" for the studied compounds, and that different types of other ligands might also fit (this was, for example, the case with GABA$_A$-targeting drugs we used in vivo and in silico experiments; docking results are not shown). In other words, one could expect these regions to be much less specific (in respect to the geometry, volume and spatial distribution of structural characters) and even unimportant for the activity (otherwise a large number of different compounds could induce channel opening). Thus, one could assume that the anxiolytic activity of the title compounds might be (at least partially) due to their strong affinity towards the GABA$_A$-BZD-binding site. Hence, it seems that the results of the in silico simulations corroborate those of the in vivo experiments. The two compounds with the highest calculated

affinity (binding energies) for the BZD-binding site were **3g** and **3h** (Fig. S6), and in vivo results pointed to **3g** as the most promising new anxiolytic (for this reason further discussion will be mainly focused on this compound). The opposite was true for **3d**, **3e** and **3k**–**m**. One should note that the length of the N-alkyl chain, or the presence/absence of a spacer between the N-atom and the aromatic core, seems to be critical for interaction with the BZD-binding pocket. One of the explanations (within the "aromatic" series) could be found in the fact that spacers confer a certain degree of conformational freedom to the molecule. Thus, critical structural features of the active molecules may adopt favorable, diazepam-like spatial arrangements. Without the spacer, the molecule is much more constrained and possibly certain structural attributes (aromatic core) cannot avoid unfavorable interactions with "forbidden" regions of the receptor (Fig. 1). A similar reasoning could be true for **3d** and **3e** (N-octyl and N-decyl derivatives).

Hit compound **3g** was docked within the BZD-binding site in a similar way as diazepam or flumazenil molecules were. The residues of the following 15 amino acids were within the 4 Å sphere (strong interactions expected) [49] around **3g**: α_1HIS101, α_1ASN102 (Loop A); α_1LYS155, α_1VAL202, α_1SER204, α_1GLY207, α_1GLU208, α_1TYR209, α_1VAL211 (Loop C); γ_2PHE77 (Loop D); γ_2ARG144 (Loop E); γ_2THR193, γ_2ARG194, γ_2SER195 and γ_2ARG197 (Loop F), Fig. 10C and D. Several residues, namely α_1HIS101, α_1VAL202, α_1SER204, α_1TYR209, α_1VAL211, γ_2PHE77, are known to be important for BZD binding [23,49]. Additional 20 residues were within a 7 Å-sphere (possible interactions) around **3g**: α_1PHE99, α_1GLY103, α_1GLU137, α_1PRO153, α_1SER158, α_1TYR159, α_1GLY200, α_1GLN203, α_1SER205, α_1THR206, α_1VAL210, α_1MET212, α_1THR213, γ_2TYR58, γ_2ASN60, γ_2THR142, γ_2GLU189, γ_2ASP192, γ_2LEU198 and γ_2TRP196. Among this, α_1TYR159 (Loop B), α_1GLY200 (Loop C), α_1SER205 (Loop C) and α_1THR206 (Loop C) are important for the binding of diazepam-type anxiolytics to the GABA$_A$ receptor [23,49].

During the design of compounds **3a**-**m**, we assumed two possible "overlay-modes" of diazepam and the title compounds (Fig. 1C and D). According to the docking results, the orientation shown in Fig. 1D was energetically (more) favorable: the ferrocene core pointed towards the same direction as did the diazepam phenyl group. This was true for both input conformers of **3g** (A and B, Fig. 4 and S6). Interestingly, despite the different overall geometries of **3g**-A and **3g**-B, the ferrocene moieties of both of them perfectly "overlapped" within the BZD-binding site. This could indicate that the ferrocene core fitted perfectly within this part of the binding pocket. In fact, the ferrocene core introduced quite unique structural features ("length", volume, hydrophobicity) to the molecule. For example, the distance between the two, (almost) parallel, aromatic Cp rings was around 3.5 Å. While one of the Cp rings was positioned in a similar manner as the diazepam phenyl group (Fig. 10 and S6), the second one enabled additional binding interactions, not possible in the case of diazepam (Fig. 10C and D).

Interestingly, F4-docking poses (interface of α_1 and β_2 subunits, Figs. 9 and 11) were positioned in the pocket that was rather analogous to the BZD-binding site: it included almost the same α_1 amino-acid residues (vicinity of α_1 Loops A, B and C).

The calculated binding energies of the most favorable F1 poses for **3g** (−8.8 kcal/mol), diazepam (−8.6 kcal/mol) and flumazenil (−8.5 kcal/mol) suggested that **3g** should have a comparable or even stronger affinity towards the GABA$_A$ receptor when compared to the mentioned two. Nevertheless, the standard anxiolytics were (slightly) more active in in vivo assays. One of the possible explanations for such discrepancy could be sought in the fact that (the most) favorable **3g** F1–F5 poses were all of comparable binding energy. This means that one could expect, under in vivo conditions, several different "F1–F5 type" ligand-receptor complexes to be formed. As it is reasonable to assume that only those with **3g** bound

to the BZD site (F1-type ligand−receptor complex) would actually enable channel opening, the active concentration of **3g** would then necessarily be much lower when compared to the nominally applied one. We could even roughly estimate the hypothetical fractional distribution of the different docking poses (and different types of ligand-receptor complexes), based on the differences in the corresponding binding energies, under the approximation that they follow the Boltzmann distribution. Under these assumptions (we approximated body temperature to be 310 K; all generated F1−F5 poses were taken into account), less than 10% of **3g** receptor associated molecules (c.a. 75% of which in the geometry that was preferred in solution) would be bound to the BZD pocket and induce channel opening. The remaining **3g**-receptor complexes would have differently oriented **3g** within F2−F5 regions and might not result in a "positive outcome" (channel opening). In other words, the majority of **3g** molecules might be bound to the receptor stronger than diazepam, but in a way that does not induce the appropriate receptor response.

3. Conclusions

Herein we reported the design, synthesis, spectral, crystallographic and electrochemical characterization of a small library of N-substituted 2-ferrocenyl-1,3-thiazolidin-4-ones (**3a**−**m**, 13 compounds in total). These compounds were designed starting from the structure of benzodiazepine-type anxiolytics, known to act via the GABA_A-BZD-binding site. Substituents introduced onto the 1,3-thiazolidin-4-one core were chosen in a way as to enable favorable interactions with the BZD-binding pocket. This turned out to be especially true for the ferrocenyl substituent, which allowed acquiring BZD-analogs with two aromatic (Cp) rings in close proximity (c.a. 3.5 Å), "positioned" in parallel. We assumed that such an arrangement would enable additional favorable interactions with the benzodiazepine-binding site. In vivo experiments (light/dark, open field, horizontal wire and diazepam-induced sleep tests; the involvement of the GABA_A-receptor complex in the activity of the most potent compound (**3g**) was evaluated using known GABA_A-targeting agents) confirmed that the designed compounds, especially 2-ferrocenyl-3-(4-methoxyphenylethyl)-1,3-thiazolidin-4-one (**3g**), possess (strong) anxiolytic properties. The docking experiments (favorable geometries of **3a-m** were inferred from crystallographic and NMR analyses) corroborated the assumptions made during the design of **3a-m** and justified the introduction of the ferrocene core into the molecules; this metallocene seems to perfectly fit into the BZD-binding site. Alongside the ferrocene core, both in vivo and in silico experiments confirmed that the introduction of CH_2-spacers between the 1,3-thiazolidin-4-one N-atom and an additional (hetero)aromatic ring was important for their activity. To the best of our knowledge, hybrids of ferrocene and 1,3-thiazolidin-4-one were not previously studied for anxiolytic properties. Thus, the herein presented data might be regarded as a start of a new chapter in the design of new thiazolidinone-ferrocene based anxiolytics. It is also reasonable to expect that further work on related ferrocene containing BZD-analogues might also result in even better GABA_A-targeting compounds.

4. Experimental section

4.1. Chemistry

4.1.1. General

All commercially available chemicals and solvents were used without further purification. TLC experiments were performed on alumina-backed silica gel 40 F254 plates (Merck, Darmstadt, Germany). The spots on TLC were visualized by UV light (254 nm) and by spraying with 50% (v/v) aqueous H_2SO_4 or phosphomolybdic acid (12 g) in EtOH (250 mL) followed by heating. Chromatographic separations were carried out using silica gel 60 (particle size distribution 40−63 μm) purchased from Merck (Darmstadt, Germany), whereas silica gel 60 on Al plates, layer thickness 0.2 mm (Merck) was used for TLC. Proton (^{1}H) and Carbon (^{13}C) NMR spectra were recorded on a Bruker Avance III 400 spectrometer (400 MHz for ^{1}H, 100 MHz for ^{13}C) and a Varian Gemini 200 spectrometer (200 MHz for ^{1}H, 50 MHz for ^{13}C). Solutions were prepared in either deuterochloroform (CDCl_3) or deuterated dimethylsulfoxide (DMSO-d_6) with chemical shifts (in ppm) referenced to TMS and/or deuterated solvent as an internal standard. 2D experiments ([1]H−^{1}H COSY, NOESY, HSQC and HMBC) were run on the Bruker Avance III 400 spectrometer with the usual pulse sequences. The IR measurements were carried out on a Perkin−Elmer Spectrum One FT-IR spectrometer using KBr disks. UV spectra (in CH_3CN) were measured using a UV-1650 PC Shimadzu spectrophotometer. High-resolution mass spectrometry (HRMS) analysis was performed using a JEOL Mstation JMS 700 instrument (JEOL, Germany). The GC/MS analyses were performed on a Hewlett−Packard 6890N gas chromatograph equipped with fused silica capillary column DB-5MS (5% phenylmethylsiloxane, 30 m × 0.25 mm, film thickness 0.25 μm, Agilent Technologies, USA) and coupled with a 5975B mass selective detector from the same company. If necessary, alongside the GC analyses, the purity was determined by high performance liquid chromatography (HPLC). HPLC was performed using an Agilent Technologies HPLC system 1200 series (Waldbronn, Germany) equipped with a quaternary pump, vacuum degasser, thermostated autosampler, thermostated column compartment and a diode array detector. Chromatographic separation was carried out using Eclipse Plus C18 column (50 mm × 4.6 mm, particle size 1.8 μm; Agilent Technologies, Waldbronn, Germany). Purity of all final compounds was 95% or higher. The microanalyses were carried out by the microanalyses service of the Institute of Organic Chemistry, Bulgarian Academy of Sciences. Cyclic voltammetry experiments were performed at room temperature in a standard three-electrode cell using an Autolab potentiostat (PGSTAT 302 N). The working electrode was a platinum disk (2 mm diameter; Metrohm). The counter electrode was a platinum wire, whereas an Ag/AgCl electrode was used as the reference. Prior to experiments, the working electrode was polished using Metrohm polishing kit 6.2802.000 (extremely fine aluminum oxide on a cloth), followed by washing with distilled water. Melting points were measured on a Mel-Temp cap. melting-points apparatus, model 1001, and the given values are uncorrected. Ultrasonic cleaner Elmasonic S 10, 30 W was used for the ultrasonically supported synthesis.

4.1.2. General procedure for the synthesis of 2-Ferrocenylthiazolidin-4-ones (**3a**−**m**)

An ice-cooled solution of the corresponding primary amine (1 mmol) and ferrocenecaboxaldehyde (214 mg, 1 mmol) in THF (2 mL) was irradiated in an ultrasonic bath for 5 min, followed by the addition of thioglycolic acid (184 mg, 2 mmol). After further irradiation for 5 min, DCC (206 mg, 1 mmol) was added to the resulting mixture and irradiation continued for another 15 min under the same conditions. DCU was removed by filtration, the solvent evaporated and the residue taken up in EtOAc (30 mL). The organic layer was washed with 5% aq. solution of citric acid, H_2O, 5% aq. solution of NaHCO_3 and brine, successively, and dried overnight (anh. Na_2SO_4). After the evaporation of the solvent, the crude mixture was purified by column chromatography (SiO_2/hexane - EtOAc 9:1, v/v).

*4.1.2.1. 3-Butyl-2-ferrocenyl-1,3-thiazolidin-4-one (**3a**).* Yield 71%, orange oil; IR (neat): ν_{max} 3094.9 (arC-H), 2957.6 ((CH$_3$)$_{as}$), 2930.9 ((CH$_2$)$_{as}$), 2871.3 ((CH$_3$)$_s$), 1669.4 (C=O), 1442.0 (δ(CH$_2$)$_{scissoring}$), 1410.0, 1377.0 (δ(CH$_3$)$_s$), 1297.0, 1105.8, 819.6; UV–Vis (CH$_3$CN): λ_{max} (log ε) 422 (2.56), 202 (4.51) nm; ^{1}H NMR (200 MHz, CDCl$_3$): δ 5.51 (br. s, 1H, N–CH–S), 4.41 (m, 1H, H–C (5′)), 4.14–4.31 (overlapping peaks, 8H, H–C (1″), H–C (2″), H–C (3″), H–C (4″), H–C (5″), H–C (2′), H–C (3′), H–C (4′)), 3.61 (AA′, 2H, SCH$_2$C=O), 3.36 (ddd, *J* = 13.8, 8.4, 5.4 Hz, 1H, CH_AH$_B$N), 2.82 (ddd, *J* = 13.8, 8.4, 5.4 Hz, 1H, CH$_A$$H_B$N), 1.11–1.40 (m, 4H, C$H_2CH_2CH_3$), 0.83 (t, *J* = 6.8 Hz, 3H, CH$_3$); ^{13}C NMR (50 MHz, CDCl$_3$): δ 170.2 (C=O), 85.1 (C (1′)), 70.0, 69.8 (C (2′), C (5′)), 69.0 (C (1″), C (2″), C (3″), C (4″), C (5″)), 68.0, 67.7 (C (3′), C (4′)), 61.3 (N–CH–S), 42.0 (CH$_2$N), 33.4 (SCH$_2$C=O), 29.0 (CH$_2$CH$_2$N), 19.9 (CH$_2$CH$_3$), 13.7 (CH$_3$); MS (EI, 70 eV) *m/z* (%): 343 [M]$^{+\cdot}$ (100), 310 (2.4), 270 (61.7), 230 (6), 213 (7.8), 199 (5.1), 186 (17.3), 166 (8.2), 148 (7.9), 121 (28.4), 97 (2.7), 77 (2.2), 56 (10.1), 41 (2.6); HRMS (ESI): *m/z* calculated for C$_{17}$H$_{21}$FeNOS+H$^+$ [M+H$^+$]: 344.07715. Found: 344.07709; Anal. Calcd for C$_{17}$H$_{21}$FeNOS: C, 59.48%; H, 6.17%; Fe, 16.27%; N, 4.08%; S, 9.34%. Found: C, 59.14%; H, 6.28%; N, 3.73%; S, 9.54%.

*4.1.2.2. 2-Ferrocenyl-3-pentyl-1,3-thiazolidin-4-one (**3b**).* Yield 78%, orange solid, mp 90 °C; IR (KBr): ν_{max} 3091.6 (arC-H), 2952.9 ((CH$_3$)$_{as}$), 2930.2 ((CH$_2$)$_{as}$), 2871.6 ((CH$_3$)$_s$), 2856.4 ((CH$_2$)$_a$), 1662.6 (C=O), 1458.7 (δ(CH$_2$)$_{scissoring}$), 1401.9, 1380.6 (δ(CH$_3$)$_s$), 1307.9, 1104.3, 1001.8, 820.2; UV–Vis (CH$_3$CN): λ_{max} (log ε) 422 (2.40), 315 (2.68), 203 (4.71) nm; ^{1}H NMR (200 MHz, CDCl$_3$): δ 5.52 (br. s, 1H, N–CH–S), 4.43 (m, 1H, H–C (5′)), 4.21–4.32 (overlapping peaks, 8H, H–C (1″), H–C (2″), H–C (3″), H–C (4″), H–C (5″), H–C (2′), H–C (3′), H–C (4′)), 3.62 (AA′, 2H, SCH$_2$C=O), 3.35 (ddd, *J* = 13.9, 8.7, 5.2 Hz, 1H, CH_AH$_B$N), 2.84 (ddd, *J* = 13.9, 8.7, 5.2 Hz, 1H, CH$_A$$H_B$N), 1.1–1.48 (m, 6H, (CH$_2$)$_3$), 0.84 (t, *J* = 6.8 Hz, 3H, CH$_3$); ^{13}C NMR (50 MHz, CDCl$_3$): δ 170.1 (C=O), 85.1 (C (1′)), 70.0, 69.8 (C (2′), C (5′)), 69.0 (C (1″), C (2″), C (3″), C (4″), C (5″)), 68.4, 67.7 (C (3′), C (4′)), 61.4 (N–CH–S), 42.3 (CH$_2$N), 33.4 (SCH$_2$C=O), 28.8, 26.6, 22.2 (CH$_2$CH$_2$CH$_2$CH$_3$), 13.9 (CH$_3$); MS (EI, 70 eV) *m/z* (%): 357 [M]$^{+\cdot}$ (100), 324 (2.8), 284 (67), 264 (1.6), 249 (2.6), 230 (6.9), 213 (10.4), 199 (6.5), 186 (18.8), 166 (8), 148 (6.6), 121 (26.4), 97 (2.5), 77 (2), 56 (7.3), 43 (3.3); HRMS (ESI): *m/z* calculated for C$_{18}$H$_{23}$FeNOS + H$^+$ [M + H$^+$]: 358.09280. Found: 358.09283; Anal. Calcd for C$_{18}$H$_{23}$FeNOS: C, 60.51%; H, 6.49%; Fe, 15.63%; N, 3.92%; S, 8.95%. Found: C, 60.83%; H, 6.64%; N, 3.64%; S, 8.80%.

*4.1.2.3. 2-Ferrocenyl-3-hexyl-1,3-thiazolidin-4-one (**3c**).* Yield 72%, yellow solid, mp 72 °C; IR (KBr): ν_{max} 3095.2 (arC-H), 2954.3 ((CH$_3$)$_{as}$), 2926.8 ((CH$_2$)$_{as}$), 2856.8 ((CH$_2$)$_s$), 1671.0 (C=O), 1441.0 (δ(CH$_2$)$_{scissoring}$), 1409.3, 1377.2 (δ(CH$_3$)$_s$), 1298.2, 1225.7, 1105.9, 1000.7, 818.2; UV–Vis (CH$_3$CN): λ_{max} (log ε) 430 (2.33), 203 (4.89) nm; ^{1}H NMR (200 MHz, CDCl$_3$): δ 5.52 (br. s, 1H, N–CH–S), 4.43 (m, 1H, H–C (5′)), 4.16–4.33 (overlapping peaks, 8H, H–C (1″), H–C (2″), H–C (3″), H–C (4″), H–C (5″), H–C (2′), H–C (3′), H–C (4′)), 3.62 (AA′, 2H, SCH$_2$C=O), 3.31 (ddd, *J* = 13.9, 8.6, 5.3 Hz, 1H, CH_AH$_B$N), 2.80 (ddd, *J* = 13.9, 8.6, 5.3 Hz, 1H, CH$_A$$H_B$N), 1.08–1.46 (m, 8H, (CH$_2$)$_4$CH$_3$), 0.85 (t, *J* = 6.5 Hz, 3H, CH$_3$); ^{13}C NMR (50 MHz, CDCl$_3$): δ 170.1 (C=O), 85.1 (C (1′)), 70.0, 69.8 (C (2′), C (5′)), 69.0 (C (1″), C (2″), C (3″), C (4″), C (5″)), 68.4, 67.7 (C (3′), C (4′)), 61.4 (N–CH–S), 42.4 (CH$_2$N), 33.4 (SCH$_2$C=O), 31.3, 26.8, 26.4 (CH$_2$CH$_2$CH$_2$CH$_2$CH$_3$), 22.4 (CH$_2$CH$_3$), 13.9 (CH$_3$); MS (EI, 70 eV) *m/z* (%): 371 [M]$^{+\cdot}$ (100), 338 (2.4), 298 (58), 263 (2.1), 240 (2.2), 213 (10.6), 199 (5.5), 186 (18.5), 166 (7.8), 148 (6.4), 121 (28.2), 97 (2.6), 77 (2), 56 (8.7), 43 (5.5); HRMS (ESI): *m/z* calculated for C$_{19}$H$_{25}$FeNOS + H$^+$ [M + H$^+$]: 372.10845. Found: 372.10840; Anal. Calcd for C$_{19}$H$_{25}$FeNOS: C, 61.46%; H, 6.79%; Fe, 15.04%; N, 3.77%; S, 8.64%. Found: C, 61.31%; H, 6.90%; N, 3.65%; S, 8.83%.

*4.1.2.4. 2-Ferrocenyl-3-octyl-1,3-thiazolidin-4-one (**3d**).* Yield 71%, yellow solid, mp 62 °C; IR (KBr): ν_{max} 3092.9 (arC-H), 2954.1 ((CH$_3$)$_{as}$), 2923.6 ((CH$_2$)$_{as}$), 2852.4 ((CH$_2$)$_s$), 1661.6 (C=O), 1440.6 (δ(CH$_2$)$_{scissoring}$), 1402.0, 1379.5 (δ(CH$_3$)$_s$), 1307.2, 1105.1, 1002.0, 821.5; UV–Vis (CH$_3$CN): λ_{max} (log ε) 422 (2.61), 329 (2.82), 203 (4.80) nm; ^{1}H NMR (200 MHz, CDCl$_3$): δ 5.52 (br. s, 1H, N–CH–S), 4.43 (m, 1H, H–C (5′)), 4.19–4.33 (overlapping peaks, 8H, H–C (1″), H–C (2″), H–C (3″), H–C (4″), H–C (5″), H–C (2′), H–C (3′), H–C (4′)), 3.62 (AA′, 2H, SCH$_2$C=O), 3.33 (ddd, *J* = 13.9, 8.6, 5.3 Hz, 1H, CH_AH$_B$N), 2.84 (ddd, *J* = 13.9, 8.6, 5.3 Hz, 1H, CH$_A$$H_B$N), 1.1–1.31 (m, 12H, (CH$_2$)$_6$CH$_3$), 0.87 (t, *J* = 6.5 Hz, 3H, CH$_3$); ^{13}C NMR (50 MHz, CDCl$_3$): δ 170.1 (C=O), 85.1 (C (1′)), 70.0, 69.8 (C (2′), C (5′)), 69.0 (C (1″), C (2″), C (3″), C (4″), C (5″)), 68.4, 67.7 (C (3′), C (4′)), 61.4 (N–CH–S), 42.4 (CH$_2$N), 33.4 (SCH$_2$C=O), 31.7, 29.1, 29.0, 26.9, 26.7 (CH$_2$CH$_2$CH$_2$CH$_2$CH$_2$CH$_2$CH$_3$), 22.6 (CH$_2$CH$_3$), 14.0 (CH$_3$); MS (EI, 70 eV) *m/z* (%): 399 [M]$^{+\cdot}$ (100), 366 (2.3), 326 (56.2), 291 (1.9), 260 (2.4), 230 (10), 213 (10.2), 199 (6.6), 186 (20.4), 166 (8.4), 148 (6), 121 (27.7), 97 (2.5), 79 (2), 56 (7.4), 41 (6.5); HRMS (ESI): *m/z* calculated for C$_{21}$H$_{29}$FeNOS + H$^+$ [M + H$^+$]: 400.13975. Found: 400.13968; Anal. Calcd for C$_{21}$H$_{29}$FeNOS: C, 63.16%; H, 7.32%; Fe, 13.98%; N, 3.51%; S, 8.03%. Found: C, 63.09%; H, 7.15%; N, 3.49%; S, 8.00%.

*4.1.2.5. 3-Dodecyl-2-ferrocenyl-1,3-thiazolidin-4-one (**3e**).* Yield 90%, yellow solid, mp 70 °C; IR (KBr): ν_{max} 2959.8 ((CH$_3$)$_{as}$), 2920.9 ((CH$_2$)$_{as}$), 2851.9 ((CH$_2$)$_a$), 1664.1 (C=O), 1466.0 (δ(CH$_2$)$_{scissoring}$), 1402.0, 1384.6 (δ(CH$_3$)$_s$), 1287.5, 1122.7; UV–Vis (CH$_3$CN): λ_{max} (log ε) 430 (2.61), 324 (2.74), 203 (4.71) nm; ^{1}H NMR (200 MHz, CDCl$_3$): δ 5.52 (br. s, 1H, N–CH–S), 4.44 (m, 1H, H–C (5′)), 4.17–4.34 (overlapping peaks, 8H, H–C (1″), H–C (2″), H–C (3″), H–C (4″), H–C (5″), H–C (2′), H–C (3′), H–C (4′)), 3.62 (AA′, 2H, SCH$_2$C=O), 3.33 (ddd, *J* = 14.0, 8.6, 5.4 Hz, 1H, CH_AH$_B$N), 2.83 (ddd, *J* = 14.0, 8.6, 5.4 Hz, 1H, CH$_A$$H_B$N), 1.04–1.41 (m, 20H, (CH$_2$)$_{10}$), 0.87 (t, *J* = 6.5 Hz, 3H, CH$_3$); ^{13}C NMR (50 MHz, CDCl$_3$): δ 170.1 (C=O), 85.2 (C (1′)), 70.0, 69.8 (C (2′), C (5′)), 69.0 (C (1″), C (2″), C (3″), C (4″), C (5″)), 68.4, 67.7 (C (3′), C (4′)), 61.4 (N–CH–S), 42.4 (CH$_2$N), 33.4 (SCH$_2$C=O), 31.8, 29.1–29.6, 26.9, 26.7 ((CH$_2$)$_9$CH$_2$CH$_3$), 22.6 (CH$_2$CH$_3$), 14.1 (CH$_3$); MS (EI, 70 eV) *m/z* (%): 455 [M]$^{+\cdot}$ (100), 422 (1.1), 382 (32.3), 347 (0.8), 310 (0.7), 288 (3.1), 230 (10.1), 213 (7.1), 199 (6.8), 186 (13.9), 166 (6.6), 148 (4.6), 121 (17.4), 97 (1.8), 69 (1.8), 55 (4.3), 43 (8.5); HRMS (ESI): *m/z* calculated for C$_{25}$H$_{37}$FeNOS + H$^+$ [M + H$^+$]: 456.20235. Found: 456.20239; Anal. Calcd for C$_{25}$H$_{37}$FeNOS: C, 65.92%; H, 8.19%; Fe, 12.26%; N, 3.08%; S, 7.04%. Found: C, 66.50%; H, 7.85%; N, 3.54%; S, 7.52%.

*4.1.2.6. 3-Hexadecyl-2-ferrocenyl-1,3-thiazolidin-4-one (**3f**).* Yield 62%, orange solid, mp 75 °C; IR (KBr): ν_{max} 3090.8 (arC-H), 2951.1 ((CH$_3$)$_{as}$), 2917.6 ((CH$_2$)$_{as}$), 2870.7 ((CH$_3$)$_s$), 2849.1 ((CH$_2$)$_a$), 1664.1 (C=O), 1464.6 (δ(CH$_2$)$_{scissoring}$), 1402.3, 1380.9 (δ(CH$_3$)$_s$), 1307.9, 1104.9, 1002.2, 823.0; UV–Vis (CH$_3$CN): λ_{max} (log ε) 441 (2.20), 324 (2.25), 203 (4.72) nm; ^{1}H NMR (200 MHz, CDCl$_3$): δ 5.52 ((br. s, 1H, N–CH–S), 4.43 (m, 1H, H–C (5′)), 4.18–4.32 (overlapping peaks, 8H, H–C (1″), H–C (2″), H–C (3″), H–C (4″), H–C (5″), H–C (2′), H–C (3′), H–C (4′)), 3.62 (AA′, 2H, SCH$_2$C=O), 3.33 (ddd, *J* = 13.8, 8.4, 5.4 Hz, 1H, CH_AH$_B$N), 2.82 (ddd, *J* = 13.8, 8.4, 5.4 Hz, 1H, CH$_A$$H_B$N), 1.03–1.39 (m, 28H, (CH$_2$)$_{14}$CH$_3$), 0.88 (t, *J* = 6.6 Hz, 3H, CH$_3$); ^{13}C NMR (50 MHz, CDCl$_3$): δ 170.1 (C=O), 85.2 (C (1′)), 70.0, 69.8 (C (2′), C (5′)), 69.0 (C (1″), C (2″), C (3″), C (4″), C (5″)), 68.5, 67.8 (C (3′), C (4′)), 61.4 (N–CH–S), 42.4 (CH$_2$N), 33.5 (SCH$_2$C=O), 31.9, 29.2–29.7, 26.9, 26.7 ((CH$_2$)$_{13}$CH$_2$CH$_3$), 22.7 (CH$_2$CH$_3$), 14.1 (CH$_3$); MS (EI, 70 eV) *m/z* (%): 511 [M]$^{+\cdot}$ (100), 478 (0.6), 438 (18.7), 397 (0.4), 366 (0.5), 344 (1.4), 324 (0.9), 287 (1.6), 260 (1.4), 230 (11), 213 (6.2), 199 (7.1), 186 (11.4), 166 (6.3), 148 (4.2), 121 (12.9), 97 (1.6), 69 (2.4), 57 (5.3), 43 (12.3); HRMS (ESI): *m/z* calculated for C$_{29}$H$_{45}$FeNOS + H$^+$ [M + H$^+$]: 512.26495. Found: 512.26501; Anal. Calcd for C$_{29}$H$_{45}$FeNOS: C,

68.08%; H, 8.87%; Fe, 10.92%; N, 2.77%; S, 6.27%. Found: C, 67.83%; H, 7.85%; N, 2.88%; S, 6.26%.

4.1.2.7. 2-Ferrocenyl-3-(4-methoxyphenethyl)-1,3-thiazolidin-4-one (3g). Yield 82%, ocher solid, mp 130 °C; IR (KBr): ν_{max} 3100.2 (arC-H), 2965.2 ((OCH$_3$)$_{as}$), 2924.1 ((CH$_2$)$_{as}$), 2837.6 ((CH$_2$)$_a$), 1667.6 (C=O), 1511.0 (arC = arC), 1458.2 (δ(CH$_2$)$_{scissoring}$), 1401.1, 1304.5 (δ(CH$_3$)$_s$), 1240.7, 1176.9, 1029.2, 817.0 (γ(arC-H)); UV−Vis (CH$_3$CN): λ_{max} (log ε) 438 (2.18), 431 (2.18), 197 (5.08) nm; MS (EI, 70 eV) *m/z* (%): 421 [M]$^{+\cdot}$(100), 388 (0.2), 348 (12.5), 314 (7.1), 287 (14.8), 255 (1.8), 226 (9), 199 (7), 186 (9.5), 166 (5.4), 148 (2.4), 135 (16.5), 121 (36.6), 105 (4.3), 91 (5.9), 77 (6.6), 65 (2), 56 (8.2), 39 (1.1); HRMS (ESI): *m/z* calculated for C$_{22}$H$_{23}$FeNOS+H$^+$ [M+H$^+$]: 406.09280. Found: 406.09286; Anal. Calcd for C$_{22}$H$_{23}$FeNOS: C, 62.71%; H, 5.50%; Fe, 13.25%; N, 3.32%; S, 7.62%. Found: C, 62.59%; H, 5.31%; N, 3.60%; S, 7.58%.

4.1.2.8. 3-Benzyl-2-Ferrocenyl-1,3-thiazolidin-4-one (3h). Yield 80%, yellow solid, mp 105 °C; IR (KBr): ν_{max} 3086.7 (arC-H), 2923.9 ((CH$_2$)$_{as}$), 1669.6 (C=O), 1495.0 (arC = arC), 1434.7 (δ(CH$_2$)$_{scissoring}$), 1399.4, 1299.3, 1105.7, 817.1, 746.3 (γ(arC-H)), 698.4; UV−Vis (CH$_3$CN): λ_{max} (log ε) 430 (2.24), 322 (2.38), 202 (4.78) nm; ^{1}H NMR (200 MHz, CDCl$_3$): δ 7.30 (overlapping peaks, 3H, H−C (3‴), H−C (4‴), H−C (5‴)), 7.13 (m, 2H, H−C (2‴), H−C (6‴)), 5.34 (br. s, 1H, N−CH−S), 4.96 (br. d, J = 15.1 Hz, 1H, CH$_A$H$_B$N), 4.41 (m, 1H, H−C (5′)), 4.27 (m, 1H, H−C (4′)), 4.15–4.23 (overlapping peaks, 6H, H−C (1″), H−C (2″), H−C (3″), H−C (4″), H−C (5″), H−C (3′)), 4.04 (dt, J = 2.2, 1.1, 1.1 Hz, 1H, H−C (2′)), 3.72 (AA′, 2H, SCH$_2$C=O), 3.61 (d, J = 15.1 Hz, 1H, CH$_A$H$_B$N); ^{13}C NMR (50 MHz, CDCl$_3$): δ 170.5 (C=O), 135.7 (C (1‴)), 128.5, 127.8 (C (2″), C (3‴), C (5‴), C (6‴)), 127.4 (C (4″)), 84.6 (C (1′)), 70.5, 69.8 (C (2′), C (5′)), 68.9 (C (1″), C (2″), C (3″), C (4″), C (5″)), 68.2, 67.6 (C (3′), C (4′)), 60.5 (N−CH−S), 45.2 (CH$_2$N), 33.3 (SCH$_2$C=O); MS (EI, 70 eV) *m/z* (%): 377 [M]$^{+\cdot}$ (100), 344 (0.8), 304 (16.4), 269 (6.8), 237 (6.5), 213 (26.4), 186 (7.9), 166 (6), 146 (6.4), 121 (25.3), 91 (21.2), 65 (4.9), 56 (10), 39 (1.3); HRMS (ESI): *m/z* calculated for C$_{20}$H$_{19}$FeNOS+H$^+$ [M+H$^+$]: 378.06150. Found: 378.06143; Anal. Calcd for C$_{20}$H$_{19}$FeNOS: C, 63.67%; H, 5.08%; Fe, 14.80%; N, 3.71%; S, 8.50%. Found: C, 63.91%; H, 4.96%; N, 3.89%; S, 8.78%.

4.1.2.9. 2-Ferrocenyl-3-furfuryl-1,3-thiazolidin-4-one (3i). Yield 99%, light orange oil; IR (neat): ν_{max} 2924.1 ((CH$_2$)$_{as}$), 1680.3 (C=O), 1503.8 (arC = arC), 1400.3, 1301.4, 1228.7, 1046.0, 1008.7, 821.5, 738.7; UV−Vis (CH$_3$CN): λ_{max} (log ε) 431 (2.28), 422 (2.39), 204 (4.82) nm; ^{1}H NMR (200 MHz, CDCl$_3$): δ 7.37 (dd, J = 1.8, 0.7 Hz, 1H, H−C (5‴)), 6.30 (dd, J = 3.2, 1.8 Hz, 1H, H−C (4‴)), 6.18 (br. d, J = 3.2 Hz, 1H, H−C (3‴)), 5.48 (br. s, 1H, N−CH−S), 4.81 (br. d, J = 15.6 Hz, 1H, CH$_A$H$_B$N), 4.43 (dt, J = 2.4, 1.3, 1.3 Hz, 1H, H−C (5′)), 4.18–4.34 (overlapping peaks, 8H, H−C (1″), H−C (2″), H−C (3″), H−C (4″), H−C (5″), H−C (2′), H−C (3′), H−C (4′)), 3.70 (d, J = 15.6 Hz, 1H, CH$_A$H$_B$N), 3.65 (AA′, 2H, SCH$_2$C=O); ^{13}C NMR (50 MHz, CDCl$_3$): δ 170.2 (C=O), 149.5 (C (2‴)), 142.3 (C (5‴)), 110.2, 108.6 (C (3‴), C (4‴)), 84.3 (C (1′)), 70.7, 69.8 (C (2′), C (5′)), 69.0 (C (1″), C (2″), C (3″), C (4″), C (5″)), 68.4, 67.6 (C (3′), C (4′)), 60.7 (N−CH−S), 38.1 (CH$_2$N), 33.2 (SCH$_2$C=O); MS (EI, 70 eV) *m/z* (%): 367 [M]$^{+\cdot}$ (100), 334 (0.3), 320 (0.3), 292 (9), 259 (3.2), 244 (5.1), 230 (9.6), 213 (28.6), 186 (7.8), 166 (4.5), 146 (2.1), 129 (6.5), 121 (26.4), 94 (2.6), 81 (21.3), 56 (10.1), 39 (1.4); HRMS (ESI): *m/z* calculated for C$_{18}$H$_{17}$FeNO$_2$S + H$^+$ [M + H$^+$]: 368.04077. Found: 368.04075; Anal. Calcd for C$_{18}$H$_{17}$FeNO$_2$S: C, 58.87%; H, 4.67%; Fe, 15.21%; N, 3.81v; S, 8.73%. Found: C, 58.59%; H, 4.73%; N, 3.68%; S, 8.53%.

4.1.2.10. 2-Ferrocenyl-3-thenyl-1,3-thiazolidin-4-one (3j). Yield 74%, yellow oil; IR (neat): ν_{max} 2924.1 ((CH$_2$)$_{as}$), 1675.8 (C=O), 1400.2, 1300.6, 1232.5, 1105.7, 1038.9, 822.9, 703.0; UV−Vis (CH$_3$CN): λ_{max} (log ε) 430 (2.32), 322 (2.33), 202 (4.89) nm; ^{1}H NMR (200 MHz, CDCl$_3$): δ 7.21 (dd, J = 5.0, 1.2 Hz, 1H, H−C (5‴)), 6.93 (dd, J = 5.0, 3.4 Hz, 1H, H−C (4‴)), 6.86 (br. d, J = 3.4 Hz, 1H, H−C (3‴)), 5.45 (br. s, 1H, N−CH−S), 4.95 (br. d, J = 15.3 Hz, 1H, CH$_A$H$_B$N), 4.43 (dt, J = 2.4, 1.2, 1.2 Hz, 1H, H−C (5′)), 4.20–4.32 (overlapping peaks, 8H, H−C (1″), H−C (2″), H−C (3″), H−C (4″), H−C (5″), H−C (2′), H−C (3′), H−C (4′)), 3.87 (d, J = 15.3 Hz, 1H, CH$_A$H$_B$N), 3.64 (AA′, 2H, SCH$_2$C=O); ^{13}C NMR (50 MHz, CDCl$_3$): δ 170.2 (C=O), 138.1 (C (2‴)), 126.8, 126.6, 125.4 (C (3‴), C (4‴), C (5‴)), 84.3 (C (1′)), 70.6, 69.9 (C (2′), C (5′)), 69.0 (C (1″), C (2″), C (3″), C (4″), C (5″)), 68.4, 67.7 (C (3′), C (4′)), 60.2 (N−CH−S), 39.9 (CH$_2$N), 33.2 (SCH$_2$C=O); MS (EI, 70 eV) *m/z* (%): 383 [M]$^{+\cdot}$ (100), 334 (0.3), 308 (11.4), 290 (1.2), 275 (6), 245 (1.6), 230 (9.2), 213 (26.3), 186 (8.3), 166 (4.7), 121 (27.8), 97 (32.7), 56 (10.4), 45 (3.4); HRMS (ESI): *m/z* calculated for C$_{18}$H$_{17}$FeNOS$_2$ + H$^+$ [M + H$^+$]: 383.01010. Found: 383.01002; Anal. Calcd for C$_{18}$H$_{17}$FeNOS$_2$: C, 56.40%; H, 4.47%; Fe, 14.57%; N, 3.65%; S, 16.73%. Found: C, 56.12%; H, 4.28%; N, 3.47%; S, 16.94%.

4.1.2.11. 2-Ferrocenyl-3-phenyl-1,3-thiazolidin-4-one (3k). Yield 61%, light orange solid, mp 146 °C; IR (KBr): ν_{max} 3099.4 (arC-H), 2909.6 ((CH$_2$)$_{as}$), 1673.8 (C=O), 1592.0 (arC = arC), 1494.9 (arC = arC), 1454.1 (δ(CH$_2$)$_{scissoring}$), 1401.9, 1276.5, 1215.8, 1025.7, 810.9, 692.1 (ϕ(arC−arC)); UV−Vis (CH$_3$CN): λ_{max} (log ε) 439 (2.19), 431 (2.18), 203 (4.92) nm; ^{1}H NMR (200 MHz, CDCl$_3$): δ 7.28 (m, 3H, overlapping peaks, H−C (3‴), H−C (4‴), H−C (5‴)), 6.96 (dd, J = 8.0, 1.7 Hz, 2H, H−C (2‴), H−C (6‴)), 5.90 (br. s, 1H, N−CH−S), 4.47 (dt, J = 2.5, 1.3, 1.3 Hz, 1H, H−C (5′)), 4.2 (tdd, J = 2.5, 1.3, 0.9 Hz, 1H, H−C (4′)), 4.15 (s, 5H, H−C (1″), H−C (2″), H−C (3″), H−C (4″), H−C (5″)), 3.99 (td, J = 2.5, 2.5, 1.3, 1H, H−C (3′)), 3.81 (AA′, 2H, SCH$_2$C=O), 3.70 (dt, J = 2.5, 1.3, 1.3 Hz, 1H, H−C (2′)); ^{13}C NMR (50 MHz, CDCl$_3$): δ 170.3 (C=O), 137.1 (C (1‴)), 129.0 (C (3‴), C (5‴)), 127.8 (C (4‴)), 127.7 (C (2‴), C (6‴)), 85.3 (C (1′)), 70.4, 69.4 (C (2′), C (5′)), 68.8 (C (1″), C (2″), C (3″), C (4″), C (5″)), 68.3, 67.2 (C (3′), C (4′)), 63.9 (N−CH−S), 33.6 (SCH$_2$C=O); MS (EI, 70 eV) *m/z* (%): 363 [M]$^{+\cdot}$ (100), 345 (0.1), 321 (2.3), 303 (0.1), 290 (34.6), 269 (3), 255 (6), 224 (15.4), 186 (10.4), 145 (4), 121 (20.2), 104 (3.5), 77 (7.8), 56 (8.9), 39 (1.1); HRMS (ESI): *m/z* calculated for C$_{19}$H$_{17}$FeNOS + H$^+$ [M + H$^+$]: 364.04585. Found: 364.04578; Anal. Calcd for C$_{19}$H$_{17}$FeNOS: C, 62.82%; H, 4.72%; Fe, 15.37%; N, 3.86%; S, 8.83%. Found: C, 53.01%; H, 4.83%; N, 3.55%; S, 8.98%.

4.1.2.12. 2-Ferrocenyl-3-(m-tolyl)-1,3-thiazolidin-4-one (3l). Yield 63%, light yellow solid, mp 138 °C; IR (KBr): ν_{max} 3079.4 (arC-H), 2920.3 ((CH$_2$)$_{as}$), 1673.8 (C=O), 1586.6 (arC = arC), 1490.8 (arC = arC), 1455.9 (δ(CH$_2$)$_{scissoring}$), 1365.1, 1300.1, 1215.7, 1106.3, 1000.1, 820.8 (γ(arC-H)), 692.4 (ϕ(arC−arC)); UV−Vis (CH$_3$CN): λ_{max} (log ε) 431 (2.23), 204 (4.96) nm; ^{1}H NMR (200 MHz, CDCl$_3$): δ 7.18 (t, J = 7.6, 7.6 Hz, 1H, H−C (5‴)), 7.05 (br. d, J = 7.6 Hz, 1H, H−C (4‴)), 6.79 (overlapping peaks, 2H, H−C (2‴), H−C (6‴)), 5.88 (br. s, 1H, N−CH−S), 4.47 (dt, J = 2.5, 1.3, 1.3 Hz, 1H, H−C (5′)), 4.21 (tdd, J = 2.5, 1.3, 0.5 Hz, 1H, H−C (4′)), 4.15 (s, 5H, H−C (1″), H−C (2″), H−C (3″), H−C (4″), H−C (5″)), 4.01 (td, J = 2.5, 2.5, 1.3, 1H, H−C (3′)), 3.81 (AA′, 2H, SCH$_2$C=O), 3.71 (dt, J = 2.5, 1.3, 1.3 Hz, 1H, H−C (2′)), 2.27 (s, 3H, CH$_3$); ^{13}C NMR (50 MHz, CDCl$_3$): δ 170.4 (C=O), 139.0 (C (1‴)), 137.1 (C (3‴)), 128.8, 128.7, 128.4, 124.8 (C (2‴), C (4‴), C (5‴), C (6‴)), 85.5 (C (1′)), 70.5, 69.4 (C (2′), C (5′)), 68.9 (C (1″), C (2″), C (3″), C (4″), C (5″)), 68.3, 67.2 (C (3′), C (4′)), 64.0 (N−CH−S), 33.6 (SCH$_2$C=O), 21.2 (CH$_3$); MS (EI, 70 eV) *m/z* (%): 377 [M]$^{+\cdot}$ (100), 359 (0.2), 335 (2.6), 319 (0.2), 304 (41.3), 283 (3.5), 269 (6.9), 238 (18.8), 214 (8.7), 182 (12.3), 166 (7.9), 152 (9.2), 121 (25.1), 91 (11.1), 77 (1.7), 56 (10.1), 39 (1.9); HRMS (ESI): *m/z* calculated for C$_{20}$H$_{19}$FeNOS + H$^+$ [M + H$^+$]: 378.06150. Found: 378.06154; Anal. Calcd for C$_{20}$H$_{19}$FeNOS: C, 63.67%; H, 5.08%; Fe, 14.80%; N, 3.71%; S, 8.50%. Found: C, 63.51%; H, 5.22%; N, 3.61%; S, 8.64%.

4.1.2.13. 2-Ferrocenyl-3-(p-tolyl)-1,3-thiazolidin-4-one (**3m**).

Yield 48%, light yellow solid, mp 154 °C; IR (KBr): ν_{max} 3072.5 (arC–H), 2922.8 ((CH$_2$)$_{as}$), 1672.0 (C=O), 1514.0 (arC = arC), 1456.8 (δ(CH$_2$)$_{scissoring}$), 1384.6 (δ(CH$_3$)$_s$), 1366.7, 1303.8, 1006.5, 1025.7, (γ(arC–H)); UV–Vis (CH$_3$CN): λ_{max} (log ε) 432 (2.26), 204 (4.85) nm; ^{1}H NMR (200 MHz, CDCl$_3$): δ 7.09 (AA'BB', J = 8.2 Hz, 2H, H–C (3''')), H–C (5''')), 6.82 (AA'BB', J = 8.2 Hz, 2H, H–C (2'''), H–C (6''')), 5.85 (br. s, 1H, N–CH–S), 4.49 (br. s, 1H, H–C (5')), 4.22 (br. s, 1H, H–C (4')), 4.17 (s, 5H, H–C (1''), H–C (2''), H–C (3''), H–C (4''), H–C (5'')), 4.03 (br. s, 1H, H–C (3')), 3.81 (AA', 2H, SCH$_2$C=O), 3.73 (br. s, 1H, H–C (2')), 2.29 (s, 3H, CH$_3$); ^{13}C NMR (50 MHz, CDCl$_3$): δ 170.5 (C=O), 137.8 (C (1''')), 134.5 (C (4''')), 129.7 (C (3'''), C (5''')), 127.6 (C (2'''), C (6''')), 85.5 (C (1')), 70.6, 69.4 (C (2'), C (5')), 68.9 (C (1''), C (2''), C (3''), C (4''), C (5'')), 68.4, 67.3 (C (3'), C (4')), 64.0 (N–CH–S), 33.6 (SCH$_2$C=O), 21.1 (CH$_3$); MS (EI, 70 eV) m/z (%): 377 [M]$^{+\cdot}$ (100), 359 (0.2), 335 (2.4), 319 (0.2), 304 (35), 283 (2.8), 269 (6.5), 238 (16.5), 214 (9.8), 182 (11.9), 166 (7.4), 152 (10.4), 121 (25.9), 91 (9.4), 77 (1.9), 56 (10.9), 39 (1.8); HRMS (ESI): m/z calculated for C$_{20}$H$_{19}$FeNOS + H$^+$ [M + H$^+$]: 378.06150. Found: 378.06152; Anal. Calcd for C$_{20}$H$_{19}$FeNOS: C, 63.67%; H, 5.08%; Fe, 14.80%; N, 3.71%; S, 8.50%. Found: C, 63.38%; H, 5.08%; N, 3.93%; S, 8.62%.

4.1.3. Crystallographic analysis

Single-crystal diffraction data for compound **3k** were collected at room temperature on an Agilent Gemini S diffractometer with graphite-monochromated MoKα radiation (λ = 71073 Å). Data reduction and empirical absorption corrections were accomplished using CrysAlisPro [52]. Crystal structure was solved by direct methods, using SIR2002 [53] and refined using SHELXL program [54]. All non-H atoms were refined anisotropically to convergence. All H atoms were placed at geometrically calculated positions with the C–H distances fixed to 0.93 from Csp^2 and 0.97 and 0.98 Å from methylene and methine Csp^3, respectively. The corresponding isotropic displacement parameters of the hydrogen atoms were equal to 1.2U$_{eq}$ and 1.5U$_{eq}$ of the parent Csp^2 and Csp^3, respectively. The crystallographic data are listed in Table 5. The PARST [55], PLATON [56] and WinGX [57] programs were used to perform geometrical calculation. Figures were produced using ORTEP-3 [58] and MERCURY, Version 2.4 [59].

4.2. Pharmacology

4.2.1. Animals and treatment

Male albino BALB/c mice (4 weeks old) weighing 20–25 g were used. The animals were kept in cages at room temperature and allowed access to food and water *ad libitum*. Fourteen hours before the start of the experiments the animals were sent to the lab and were given only water. The experiments were performed, in accordance with the declaration of Helsinki and European Community guidelines for the ethical handling of laboratory animals (EEC Directive of 1986; 86/609/EEC) and the related ethics regulations of our University (01-2857-4). Experimental groups consisted of 6 animals and all animals were injected intraperitoneally (ip) with experimental substances (25, 50 and 100 mg/kg) or with control substances (diazepam (Hemofarm, Vršac, Serbia), 2 mg/kg, or olive oil, 10 mL/kg), 1 h before the commencement of each experiment.

4.2.2. Light/dark (LD) test

The light/dark transition (the apparatus was a box of the following dimensions: 40 cm × 60 cm × 20 cm) was used as the test of unconditioned anxiety. The apparatus had two chambers connected by a round opening (7.0 cm) located at floor level, in the center of the dividing wall, by which mice could cross between the chambers. A larger chamber was white and illuminated by a 60 W

Table 5
Crystallographic data for crystal structure of **3k**.

Empirical formula	C19 H17 Fe N O S
Formula weight	363.25
Color, crystal shape	Orange, prism
Crystal size (mm^3)	0.35 × 0.19 × 0.15
Temperature (K)	293 (2)
Wavelength (Å)	0.71073
Crystal system	Monoclinic
Space group	P2$_1$/n
Unit cell dimensions	
a (Å)	9.0589 (4)
b (Å)	5.8848 (3)
c (Å)	29.7237 (13)
α (°)	90
β (°)	96.106 (4)
γ (°)	90
V (Å^3)	1575.58 (13)
Z	4
D$_{calc}$ (Mg/m^3)	1.531
μ (mm^{-1})	1.092
θ range for data collection (°)	2.90 to 29.00
Reflections collected	7006
Independent reflections, R$_{int}$	3594, 0.0260
Completeness to θ = 26.00°	99.9
Data/restraints/parameters	3594/0/208
Goodness-of-fit on F^2	1.067
Final R$_1$/wR$_2$ indices (I > 2σ_I)	0.0458, 0.0849
Final R$_1$/wR$_2$ indices (all data)	0.0651, 0.0921
Largest diff. peak and hole (e Å^{-3})	0.252 and −0.366

bulb, whereas the smaller compartment was black and not illuminated at all. Each animal was placed at the center of the illuminated compartment, facing away from the round passage. The time spent in illuminated and dark places, time of the first crossing (transition), as well as the number of entries in each space, was recorded for 5 min [47].

4.2.3. Open field (OF) test

In order to detect any association to immobility in the tests and changes in motor activity, the OF apparatus was used. The studies were carried out on mice according to a method previously described [47]. The floor of the apparatus was divided into twenty-five equal (10 × 10 cm) squares. Mice were placed individually into the corner of the arena and allowed to explore it freely. Behavior scores included the frequency of ambulation (the number of crossing sector lines with all four paws) and rearing (number of times mouse stood on its hind limbs).

4.2.4. Horizontal wire (HW) test

The HW test was used to assess a compound's effects on the muscle tone of mice. The test apparatus was based on that described earlier [47]. The number of animals that were unable to grasp a horizontal wire, with either the forepaws, or at least with one hindpaw within 10 s was recorded.

4.2.5. Involvement of the GABA receptor complex in anxiolytic activity of compound 3g

The involvement of GABA$_A$-receptor complexes was evaluated by experiments that included the application of a competitive antagonist Flumazenil (FLU; Sigma–Aldrich, St. Louis, Missouri, USA). Three groups of mice (6 per group) were given FLU (15 min before other substances) as an ip injection (3 mg/kg) and afterwards the animals were treated as follows: group I (negative control group) received vehicle (olive oil) in a dose of 10 mL/kg, group II (positive control group) received diazepam in a dose of 1 mg/kg and group III (experimental) received compound **3g** in a dose of 50 mg/

kg [45]. After the treatments the animals were submitted to a LD test.

A second set of experiments served to evaluate the interaction of compound **3g** with the picrotoxin GABA$_A$-receptor-binding site. An ip dose of a non-competitive antagonist picrotoxin (PIC, 1 mg/kg; Tokyo Chemical Industry, Tokyo, Japan) administered 15 min before other substances was used in this sense [60,61]. The treatments of positive and negative controls, as well as the experimental groups, were same as described in the previous paragraph. After the treatments the animals were submitted to a LD test.

4.2.6. Diazepam-induced sleep

Sleep inducing or potentiating effects of the synthesized library compounds were investigated in experiments where a 20 mg/kg dose (ip) of diazepam was used to induce sleep in mice. The time required to induce loss of the righting reflex was defined as sleep latency, while the time that elapsed between the loss and recovery of the righting reflex was considered sleeping time [47].

4.2.7. Anticonvulsant activity

The influence of **3g** on convulsions induced by pentylenetetrazol (PTZ; Alfa Aesar GmbH & Co KG, Karlsruhe, Germany) and isoniazid (ISN; Tokyo Chemical Industry, Tokyo, Japan) was studied [48]. One hour before PTZ (70 mg/kg) or INH (250 mg/kg) injections, the animals were ip treated with vehicle (olive oil, 10 mL/kg), **3g** (50 mg/kg) or diazepam (1 mg/kg). After the PTZ application the onset of seizures (sec) and occurrence of hind-limb tonic extensions (sec) were recorded, whereas in ISN treated animals the seizure onset (min) and % of living mice in 30 min were monitored.

4.3. Statistical analysis

Results were expressed as the mean ± SD. Statistically significant differences were determined by one-way analysis of variance (ANOVA) followed by Tukey's post hoc test for multiple comparisons (Graphpad Prism version 5.03, San Diego, CA, USA). Probability values (p) less than 0.05 were considered to be statistically significant.

4.4. Docking experiments

All library compounds were docked in the extracellular domain of the unified homology model of the $\alpha_1\beta_2\gamma_2$ GABA$_A$ receptor, primarily based on the glutamate-gated chloride channel [23]. This was also done for diazepam, flumazenil, isoniazid, tetrazole, picrotoxinin and picrotin, which were used in the biological *in vivo* tests. All docking experiments were performed using AutoDock Vina 1.1.2 software, as blind dockings [62]. Extracellular domain of the receptor was divided into four partially overlapping grid boxes (GB1-GB4), that were together large enough to encompass any possible ligand—receptor complex. The centers of grid boxes were at *x*, *y*, z = 27.479, 66.798, 76.015 (GB1); 27.479, 66.798, 52.838 (GB2); −6.757, 66.798, 49.491 (GB3); −6.757, 66.798, 81.154 (GB4) (Figure S7, Supporting Information); the size of each individual search space (volume of the grid box) was set to be 46 × 76 × 54 Å. Autodock Vina docking was performed using exhaustiveness value of 500, while the number of search modes was set to 20. All other parameters were used as defaults. The ligands were allowed to flexibly dock, but the receptor backbone and side chains remained rigid during the docking. For all library compounds, two different input conformations (these corresponding to the preferred geometries found in solid state and solution and were inferred from crystallographic and NMR analyses), generated by HyperChem 8.0 Software and minimized using molecular mechanics MM + force field, were used. The validity of the docking results was confirmed by AutoDock Vina ability to accurately predict the diazepam-binding site, consistent with the available experimental data [23,49]. Autodock Tools version 1.5.6 was used to convert the ligand and receptor molecules to proper file formats (pdbqt) for AutoDock Vina docking. The same program was used for the visualization of docking results [63]. The output pdbqt files for the preferred BZD-docking poses of the most active compound (**3g**, *in vivo* experiments) are given in Supporting Information. All *in silico* experiments were run using Intel® Core™ i7-3930K 3.20 GHz Six core unlocked CPU Processor.

Transparency declarations

The authors declare no conflict of interest.

Acknowledgments

Appendix A. Supplementary data

Supplementary data related to this article can be found at http://dx.doi.org/10.1016/j.ejmech.2014.05.062.

References

[1] L.N. Ravindran, M.B. Stein, The pharmacologic treatment of anxiety disorders: a review of progress, J. Clin. Psychiatr. 71 (2010) 839—854.
[2] G. Griebel, A. Holmes, 50 years of hurdles and hope in anxiolytic drug discovery, Nat. Rev. Drug. Discov. 12 (2013) 667—687.
[3] B. Saraceno, Advancing the global mental health agenda, Int. J. Public Health 3 (2007) 140—141.
[4] S. Taliani, B. Cosimelli, F. Da Settimo, A.M. Marini, C. La Motta, F. Simorini, S. Salerno, E. Novellino, G. Greco, S. Cosconati, L. Marinelli, F. Salvetti, G. L'Abbate, S. Trasciatti, M. Montali, B. Costa, C. Martini, Identification of anxiolytic/nonsedative agents among Indol-3-ylglyoxylamides acting as functionally selective agonists at the γ-aminobutyric acid-a (GABA$_A$) α_2 benzodiazepine receptor, J. Med. Chem. 52 (2009) 3723—3734.
[5] Q. Wang, Y. Han, H. Xue, Ligands of the GABA$_A$ receptor benzodiazepine binding site, CNS Drug. Rev. 5 (1999) 125—144.
[6] G.A.R. Johnston, GABA$_A$ receptor channel pharmacology, Curr. Pharm. Des. 11 (2005) 1867—1885.
[7] Q. Huang, X. He, C. Ma, R. Liu, S. Yu, C.A. Dayer, G.R. Wenger, R. McKernan, J.M. Cook, Pharmacophore/receptor models for GABA$_A$/BzR subtypes ($\alpha_1\beta_3\gamma_2$, $\alpha_5\beta_3\gamma_2$, and $\alpha_6\beta_3\beta_2$) via a comprehensive ligand-mapping approach, J. Med. Chem. 43 (2000) 71—95.
[8] M. Mula, S. Pini, G.B. Cassano, The role of anticonvulsant drugs in anxiety disorders: a critical review of the evidence, J. Clin. Psychopharmacol. 27 (2007) 263—272.
[9] A.K. Jain, A. Vaidya, V. Ravichandran, S.K. Kashaw, R.K. Agrawal, Recent developments and biological activities of thiazolidinone derivatives: a review, Bioorg. Med. Chem. 20 (2012) 3378—3395.
[10] W. Cunico, C.R.B. Gomes, W.T. Vellasco Jr., Chemistry and biological activities of 1,3-Thiazolidin-4-ones, Mini-Rev. Org. Chem. 5 (2008) 336—344.
[11] A. Verma, S.K. Saraf, 4-Thiazolidinone — a biologically active scaffold, Eur. J. Med. Chem. 43 (2008) 897—905.
[12] S.P. Singh, S.S. Parmar, K. Raman, V.I. Stenberg, Chemistry and biological activity of thiazolidinones, Chem. Rev. 81 (1981) 175—203.
[13] K.N.M. Daeffler, H.A. Lester, D.A. Dougherty, Functionally important aromatic—aromatic and sulfur-π; interactions in the D2 dopamine receptor, J. Am. Chem. Soc. 134 (2012) 14890—14896.
[14] D. Ilić, I. Damljanović, D. Stevanović, M. Vukićević, P. Blagojević, N. Radulović, R.D. Vukićević, Sulfur-containing ferrocenyl alcohols and oximes: new promising antistaphylococcal agents, Chem. Biodivers. 9 (2012) 2236—2253.
[15] D.Z. Ilić, I.S. Damljanović, D.D. Stevanović, M.D. Vukićević, N.S. Radulović, V. Kahlenberg, G. Laus, R.D. Vukićević, Synthesis, spectral characterization, electrochemical properties and antimicrobial screening of sulfur containing acylferrocenes, Polyhedron 29 (2010) 1863—1869.
[16] A.Z. Pejović, I.S. Damljanović, D.D. Stevanović, M.D. Vukićević, S.B. Novaković, G.A. Bogdanović, N.S. Radulović, R.D. Vukićević, Antimicrobial ferrocene containing quinolinones: synthesis, spectral, electrochemical and structural characterization of 2-Ferrocenyl-2,3-dihydroquinolin-4(1H)-one and its 6-Chloro and 6-Bromo derivatives, Polyhedron 31 (2012) 789—795.

[17] I. Damljanović, D. Stevanović, P. Pejović, M. Vukićević, S.B. Novaković, G.A. Bogdanović, T. Mihajlov-Krstev, N. Radulović, R.D. Vukićevi&cacute, Antibacterial 3-(Arylamino)-1-ferrocenylpropan-1-ones: synthesis, spectral, electrochemical and structural characterization, J. Org. Chem. 696 (2011) 3703–3713.

[18] Z.R. Ratković, Z.D. Juranić, T.P. Stanojković, D.D. Manojlović, R.D. Vukićević, N.S. Radulović, M.D. Joksović, Synthesis, characterization, electrochemical studies and antitumor activity of some new chalcone analogues containing ferrocenyl pyrazole moiety, Bioorg. Chem. 38 (2010) 26–32.

[19] M.D. Joksović, V.R. Marković, Z.D. Juranić, T.P. Stanojković, LJ.S. Jovanović, I.S. Damljanović, K.F. Mesaros-Secenji, N.M. Todorović, S.S. Trifunović, R.D. Vukićević, Synthesis, characterization and antitumor activity of novel n-substituted alpha-amino acids containing ferrocenyl pyrazole-moiety, J. Org. Chem. 694 (2009) 3935–3942.

[20] I.S. Damljanović, M.D. Vukićević, N.S. Radulović, R.M. Palić, E. Ellmerer, Z.R. Ratković, M.D. Joksović, R.D. Vukićević, Synthesis and antimicrobial activity of some new pyrazole derivatives containing a ferrocene unit, Bioorg. Med. Chem. Lett. 19 (2009) 1093–1096.

[21] C. Biot, G. Glorian, LA. Maciejewski, J.C. Brocard, Synthesis and antimalarial activity in Vitro and in vivo of a new ferrocene-chloroquine analogue, J. Med. Chem. 40 (1997) 3715–3718.

[22] P. Beagley, M.A.L. Blackie, K. Chibale, C. Clarkson, R. Meijboom, J.R. Moss, P.J. Smith, H. Su, Synthesis and antiplasmodial activity in vitro of new ferrocene-chloroquine analogues, Dalt. Trans. (2003) 3046–3051.

[23] N. Metzler-Nolte, U. Schatzschneider, Bioinorganic Chemistry: a Practical Course, Walter de Gruyter GmbH & Co KG, Berlin, 1990.

[24] R. Bergmann, K. Kongsbak, P.L. Sorensen, T. Sander, T.A. Balle, Unified model of the $GABA_A$ receptor comprising agonist and benzodiazepine binding sites, Plos One 8 (2013) e52323.

[25] F.C. Brown, 4-Thiazolidinones, Chem. Rev. 61 (1961) 463–521.

[26] H. Erlenmeyer, V. Oberlin, Zur Kenntnis der Thiazolidone-(4), Hel. Chim. Acta 30 (1947) 1329–1335.

[27] A.R. Surrey, The Preparation of 4-Thiazolidones by the reaction of thioglycolic acid with Schiff bases, J. Am. Chem. Soc. 69 (1947) 2911–2912.

[28] K.M. Hassan, Studies on ferrocenes and its derivatives, VI. Cyclocondensation reaction of some ferrocenyl Anils, Z. Naturforsch 33b (1978) 1508–1514.

[29] R.K. Rawal, R. Tripathi, S. Kulkarni, R. Paranjape, S.B. Katti, C. Pannecouque, E. De Clercq, 2-(2,6-Dihalo-Phenyl)-3-Heteroaryl-2-ylmethyl-1,3-Thiazolidin-4-ones: Anti-HIV agents, Chem. Biol. Drug. Des. 72 (2008) 147–154.

[30] R.K. Rawal, T. Srivastava, W. Haq, S.B. Katti, An expeditious synthesis of thiazolidinones and tetathiazanones, J. Chem. Res. 5 (2004) 368–369.

[31] T. Srivastava, W. Haq, S.B. Katti, Carbodiimide Mediated synthesis of 4-Thiazolidinones by one-pot three-component condensation, Tetrahedron 58 (2002) 7619–7624.

[32] C.R.J. Woolston, J.B. Lee, F.J. Swinbourne, An infra-red Spectroscopic study of some substituted 1,3-Thiazolidin-4-ones, Phosphorus Sulfur 78 (1993) 223–235.

[33] C.R.J. Woolston, J.B. Lee, F.J. Swinbourne, W.A. Thomas, Proton NMR Investigation of some substituted 1,3-Thiazolidin-4-ones, Mag. Reson. Chem. 30 (1992) 1075–1078.

[34] J. Tierney, D. Sheridan, K. Kovalesky, Substituent effects for some substituted 3-Benzyl-2-phenyl-1,3-thiazolidin-4-ones using ^{1}H and ^{13}C NMR, Heterocycl. Commun. 6 (2000) 105–112.

[35] C.R.J. Woolston, J.B. Lee, F.J. Swinbourne, Carbon-13 NMR Investigation of some substituted 1,3-Thiazolidin-4-ones, Mag. Reson. Chem. 31 (1993) 348–351.

[36] C.R.J. Woolston, J.B. Lee, F.J. Swinbourne, The effects of ring modification on the mass spectrometric fragmentation of some 2,3-Diaryl-1,3-thiazolidin-4-ones under electron impact, Phosphorus Sulfur 97 (1994) 157–163.

[37] G. Innorta, F. Scagnolari, A. Modelli, S. Torroni, A. Foffani, S. Sorriso, A Reinvestigation of the mass spectra of substituted ferrocenes: Accurate fragmentation Pathways and Ionic structures by analysis of Metastable ion spectra, J. Org. Chem. 241 (1983) 375–383.

[38] D. Hickel, J.M. Leger, A. Carpy, M.G. Vigorita, A. Chimirri, S. Grasso, Structure of 3-(2-Pyridyl)-2-(2-tolyl)-1,3-thiazolidin-4-one, $C_{15}H_{14}N_2OS$, Acta Crystallogr. C. 39 (1983) 240–246.

[39] M. Bourinn, M. Hascoet, B. Mansouri, M.C. Colombel, X. Bradwejn, Comparison of behavioral effects after single and repeated administration of four benzodiazepines in three mice behavioral models, J. Psychiatr. Neurosci. 17 (1992) 72–77.

[40] R.J. Blanchard, K.J. Flannelly, D.C. Blanchard, Defensive behaviour of laboratory and wild Rattus norvegicus, J. Comp. Psychol. 100 (1986) 101–107.

[41] S.K. Bhattacharya, K.S. Satyan, Experimental methods for evaluation of psychotropic agents in rodents: I-antianxiety agents, Indian J. Exp. Biol. 35 (1997) 565–575.

[42] G.R.M. Perez, I.J.A. Perez, D. Garcia, M.H. Sossa, Neuropharmacological activity of Solanum nigrum Fruit, J. Ethnopharmacol. 62 (1998) 43–48.

[43] F. Crestani, K. Löw, R. Keist, M.J. Mandelli, H. Möhler, U. Rudolph, Molecular targets for the myorelaxant action of diazepam, Mol. Pharmacol. 59 (2001) 442–445.

[44] M. Bourin, M. Hascoët, The mouse light/dark box test, Eur. J. Pharmacol. 463 (2003) 55–65.

[45] O. Grundmann, J.I. Nakajima, S. Seo, V. Butterweck, Anti-anxiety effects of Apocynum venetum L. in the elevated plus Maze test, J. Ethnopharmacol. 110 (2007) 406–411.

[46] S.E. File, R.G. Lister, Do the reductions in Social interactions produced by picrotoxin and pentylenetetrazol indicate Anxiogenic actions, Neuropharmacology 23 (1984) 793–796.

[47] N.S. Radulović, A.B. Miltojević, P.J. Randjelović, N.M. Stojanović, F. Boylan, Effects of methyl and isopropyl N-methylanthranilates from Choisya ternata Kunth (Rutaceae) on experimental anxiety and depression in mice, Phytother. Res. 27 (2013) 1334–1338.

[48] E. Ngo Bum, M. Schmutz, C. Meyer, A. Rakotonirina, M. Bopelet, C. Portet, A. Jeker, S.V. Rakotonirina, H.R. Olpe, P. Herrling, Anticonvulsant properties of the methanolic extract of Cyperus articulatus (Cyperaceae), J. Ethnopharmacol. 76 (2001) 145–150.

[49] S.M. Hanson, E.V. Morlock, K.A. Satyshur, C. Czajkowski, Structural requirements for eszopiclone and Zolpidem binding to $GABA_A$ receptor are different, J. Med. Chem. 51 (2008) 7243–7252.

[50] T.S. Carpenter, E.Y. Lau, F.C. Lightstone, Identification of possible secondary picrotoxin-binding site on the $GABA_A$ receptor, Chem. Res. Toxicol. 26 (2013) 1444–1454.

[51] O. Trott, A.J. Olson, AutoDock Vina: improving the speed and accuracy of docking with a new scoring function, efficient optimization, and multi-threading, J. Comput. Chem. 31 (2010) 455–461.

[52] Agilent, CrysAlis PRO, Agilent Technologies, Yarnton, Oxfordshire, England, 2013.

[53] M.C. Burla, M. Camalli, B. Carrozzini, G.L. Cascarano, C. Giacovazzo, G. Polidori, R. Spagna, SIR2002: the program, J. Appl. Crystallogr. 36 (2003) 1103.

[54] G.M. Sheldrick, A short history of SHELX, Acta Crystallogr. A 64 (2008) 112–122.

[55] M. Nardelli, PARST95-an update to PARST: a system of Fortran routines for calculating molecular structure parameters from the results of crystal structure analyses, J. Appl. Crystallogr. 28 (1995) 659.

[56] A.L. Spek, Single-crystal structure validation with the program PLATON, J. Appl. Crystallogr. 36 (2003) 7–13.

[57] L.J. Farrugia, WinGX Suite for small-molecule single-crystal crystallography, J. Appl. Cryst. 32 (1999) 837–838.

[58] L.J. Farrugia, WinGX and ORTEP for windows: an update, J. Appl. Crystallogr. 45 (2012) 849–854.

[59] C.F. Macrae, P.R. Edgington, P. McCabe, E. Pidcock, G.P. Shields, R. Taylor, M. Towler, J. van de Streek, Mercury: visualization and analysis of crystal structures, J. Appl. Crystallogr. 39 (2006) 453–457.

[60] J.F. Rodríguez-Landa, J.D. Hernández-Figueroa, B.C. Hernández-Calderón, M. Saavedra, Anxiolytic-like effect of phytoestrogen genistein in rats with long-term absence of ovarian hormones in the black and white model, Prog. Neuro-psychoph. 33 (2009) 367–372.

[61] I.P. Barettaa, R.A. Felizardo, V.F. Bimbato, M.G.J. dos Santos, C.A.L. Kassuya, J.A. Gasparotto da Silva, S.M. de Oliveira, J. Ferreira, R. Andreatini, Anxiolytic-like effects of acute and chronic treatment with Achillea millefolium L. Extract, J. Ethnopharmacol. 140 (2012) 46–54.

[62] N. Rnjan, K.F. Andreasen, S. Kumar, D. Hyde-Volpe, D.P. Arya, Aminoglycoside binding of Oxytricha nova telomeric DNA, Biochemistry 49 (2010) 9891–9903.

[63] M.F. Sanner, Python: a programming language for software integration and development, J. Mol. Graph. Model. 17 (1999) 57–61.